Long-range transport of Saharan dust over northwestern Europe during EUCAARI 2008 campaign: Evolution of dust optical properties by scavenging

Nelson Bègue, Pierre Tulet, Jean-Pierre Chaboureau, Gregory Roberts, Laurent Gomes, Marc Mallet

Long-range transport of Saharan dust over northwestern Europe during EUCAARI 2008 campaign: Evolution of dust optical properties by scavenging

N. Bègue,[1] P. Tulet,[1] J.-P. Chaboureau,[2] G. Roberts,[3] L. Gomes,[3,4] and M. Mallet[2]

Received 13 February 2012; revised 12 July 2012; accepted 15 July 2012; published 5 September 2012.

[1] The evolution of dust optical properties is illustrated in this paper through a case of long-range transport of Saharan dust over northwestern Europe during the European Integrated Project on Aerosol-Cloud-Climate and Air Quality Interactions (EUCAARI) experimental campaign in 2008. This spread of dust over northwestern Europe is investigated by combining satellite, airborne, ground-based observations and the non-hydrostatic meso-scale model Meso-NH. The total dust amount emitted during the study period is estimated to 185 Tg. The analysis of the removal processes reveals that only 12.5 Tg is lost by dry deposition, and that wet deposition is the main process of dust removal (73 Tg). The observed aerosol optical thickness ranged from 0.1 to 0.5 at the wavelength of 440 nm, with a maximum value close to 1 is found over the Netherlands (51.97°N, 4.93°E). Over that site, the main dust layer is located between 2.5 and 5.2 km above sea level (asl), moreover dust was also present at 0.9 km asl. The nephelometer measurements on board the ATR-42 aircraft revealed a strong wavelength dependence of the scattering coefficient over the Netherlands. The Angström exponent is greater than 0.5, whereas usually it approaches zero in presence of Saharan dust. This is due to high precipitation scavenging efficiency for the coarse mode, particularly below 4 km. Our results confirm that atmospheric conditions govern the life cycle of dust microphysical phenomena, providing conditions for transformation processes during transport, and removal of particles from the atmosphere.

Citation: Bègue, N., P. Tulet, J.-P. Chaboureau, G. Roberts, L. Gomes, and M. Mallet (2012), Long-range transport of Saharan dust over northwestern Europe during EUCAARI 2008 campaign: Evolution of dust optical properties by scavenging, *J. Geophys. Res.*, *117*, D17201, doi:10.1029/2012JD017611.

1. Introduction

[2] Dust aerosols are well known for the role they can play in modulating the climate system at local and global scales. Mineral dust contributes significantly to the global radiative budget through absorption and scattering of longwave and shortwave radiation [*Intergovernmental Panel on Climate Change*, 2001]. Airborne dust generally increases (except above high surface albedo) upward flux in the shortwave and decrease them in the longwave [*Mallet et al.*, 2009]. In a cloudy environment, dust enhances the concentration of cloud droplets and influences their size, thus changes the potential of clouds to produce rain [*Rosenfeld et al.*, 2002]. Numerical models which simulate dust emission, transport and deposition are important tools to quantify dust fluxes and the associated climate impact [*Todd et al.*, 2008]. Moreover, aerosol satellite data have been helpful to locate and to study the variability of the major dust source [*Caquineau et al.*, 2002; *Herman et al.*, 1997; *Prospero et al.*, 2002].

[3] The African continent, especially its northern part, hosts the main sources of dust on the earth. It is the combination of sources rich in erodible material, energetic wind systems, and a coupling to wind system that facilitate long-range transport. Estimated annual dust emission for North Africa ranges from 170 to 1600 Tg yr^{-1} [*Engelstaedter et al.*, 2006]. The dust emitted by the North African sources affect many adjacent continental and ocean/sea regions [*Engelstaedter et al.*, 2006; *Prospero et al.*, 2002]. The bulk of the dust is transported westward into the Atlantic Ocean [*Barkan et al.*, 2004] and the Gulf of Guinea with the strong northerlies prevailing in the summer time [*Koren et al.*, 2003]. However, a part of dust is also transported northward across the Mediterranean into southern and central Europe [*Collaud Coen et al.*, 2004; *Hamonou et al.*, 1999; *Papayannis et al.*, 2008]. Overall, the two main features that influence the dust transport from Africa

[1]Laboratoire de l'Atmosphere et des Cyclones, UMR 8105 CNRS, Universite de la Réunion, Saint-Denis, France.
[2]Laboratoire d'Aérologie, University of Toulouse III and CNRS, Toulouse, France.
[3]CNRM/GAME, URA 1357, CNRS - Météo-France, Toulouse, France.
[4]Deceased 10 February 2012.

Corresponding author: N. Bègue, Laboratoire de l'Atmosphere et des Cyclones, UMR 8105 CNRS, Universite de la Réunion, Avenue Rene Cassin, FR-97715 Saint-Denis, France. (nelson.begue@univ-reunion.fr)

0148-0227/12/2012JD017611

into Europe is the trough that emanates from the Icelandic low-pressure southward and the subtropical high over northern Africa. The strength and position of these two systems define the direction and the potential to carry dust northward into the Mediterranean [*Barkan et al.*, 2005]. In extreme cases the dust can reach the northern Europe, reaching the shores of the Baltic Sea [*Ansmann et al.*, 2003; *Franzen et al.*, 1994; *Reiff et al.*, 1986].

[4] Atmospheric conditions govern the life cycle of dust microphysical phenomena, providing conditions for transformation processes during transport, and removal of particles from the atmosphere. Thus, depending on travel distance and residence time over source regions and monitoring site, the physical and chemical properties of dust can be modified, which, in turn, changes the dust's optical properties [*Perrone et al.*, 2005]. Based on lidar observations over Thessaloniki (40.65°N; 22.90°E), *Balis et al.* [2004] found that the mixing of dust with anthropogenic particles during their transport changes the dust optical characteristics, and thus, makes difficult to distinguish the dust particles from those of urban origin. The variations of optical parameters with wavelength reflect changes in the physico-chemical properties and size distribution of particles [*Israelevich et al.*, 2003], we use these properties to study a case of dust transport over Europe.

[5] Long-range transport of Saharan dust to the northern parts of Europe was observed during the European Integrated Project on Aerosol-Cloud-Climate and Air Quality Interactions (EUCAARI) experimental campaign in 2008 [*Kulmala et al.*, 2009]. From 25 to 31 May 2008, a major Saharan dust event occurred and the dust plume reached the shores of the Baltic Sea. *Hamburger et al.* [2011] reported on the synoptic and pollution situation over Europe in May 2008, through the use of the meteorological analysis and airborne measurements. Their analysis reveals that the second half of May was characterized by westerly flow and the passage of a frontal systems with strong convective activity and heavy precipitation over central Europe. This dust event was studied by *Pappalardo et al.* [2010] for showing first results in terms of comparison between the lidar measurements obtained from Cloud-Aerosol Lidar and Infrared Pathfinder Satellite Observation (CALIPSO) and the European Aerosol Research Lidar NETwork(EARLINET). *Pappalardo et al.* [2010] conducted a statistical analysis of dust properties over Italian and German regions. They found typical Angström exponent and lidar ratio values at 355 nm on the order of 0.15 and 49 $\pm$ 10 sr, respectively.

[6] The analysis of the dust properties over the Netherlands, however, was not considered by *Pappalardo et al.* [2010], even though the dust plume reached the Netherlands where Aerosol Optical Thickness (AOT) close to 1 was observed. The measurements obtained during the EUCAARI campaign reveal a strong wavelength dependence of the scattering coefficient, whereas the dust optical parameters are usually significantly less dependent on wavelength. Thus, questions arise about the evolution of the dust optical properties over the Netherlands. In this paper, we examine first the characteristics of this dust Saharan event through a quantitative evaluation of the dust transport. In a second step, we examine and discuss the influence of the atmospheric conditions on the evolution of the dust optical properties during their transport from the Sahara region to the Netherlands. We focus particularly on the impact of the precipitation on the dust size distribution, and its consequences on the evolution of the dust optical properties.

[7] The paper is organized as follows: Section 2 describes the observations and the model used for the investigation of this dust transport; Section 3 presents the characteristics of the Saharan dust event; Section 4 gives a quantitative evaluation of the dust transport; an analysis of the dust plume properties over the Netherlands is provided in Section 5; and the summary and the conclusions are given in Section 6.

2. Observations and Model Description

2.1. Observations

[8] In May 2008, an intensive experimental campaign combining airborne, in-situ and remote sensing measurements called EUCAARI-IMPACT (where IMPACT stands for Intensive Observation Period at Cabauw Tower) was performed using the French ATR-42 [*Crumeyrolle et al.*, 2010]. The aerosol light scattering were measured by an integrating nephelometer (model TSI 3563, TSI Inc., St Paul, MN) aboard the F-ATR-42 aircraft. The design, calibration and performance evaluation of this device are discussed in details by *Anderson et al.* [1996]. It is worth to note that the measured aerosol light scattering coefficients were corrected for artifacts from truncation and the non-Lambertian light source in the nephelometer following the method presented by *Anderson and Ogren* [1998]. The aerosol instrumentation has been connected to the ATR community aerosol inlet (CAI), which is designed for the ATR to allow isokinetic and isoaxial sampling relative to the incoming air stream. The cut diameter for the CAI is 5 μm. This isokinetic and isoaxial inlet has a 50% sampling efficiency for particle size higher than 5 μm [*Crumeyrolle et al.*, 2008, 2010].

[9] During this intensive experimental campaign, the Cabauw Experimental Site for Atmospheric Research (CESAR, 51.97°N, 4.93°E) was selected as a supersite to quantify the regional aerosol properties including aerosol formation, transformation, transport and deposition [*Kulmala et al.*, 2009]. We used observations from the ALS-450 UV-lidar manufactured by Leosphere, which has been operated by the Royal Netherlands Meteorological Institute (KNMI) at CESAR since 2007. This instrument enables the retrieval of aerosol optical properties (extinction, backscatter coefficient and depolarization ratio) at 353 nm between 100 m and 20 km with a vertical resolution of 15 m [*Raut and Chazette*, 2009]. During this intensive observational period, the lidar operated continuously.

[10] The ground sites selected to evaluate the temporal evolution of the dust plume are composed of the AErosol RObotic NETwork (AERONET) sites at Cabauw, Helgoland (54.43°N, 7.89°E), Kanzelhohe (46.68°N, 13.91°E) and Lecce (40.34°N, 18.11°E). The measurements are routinely monitored using a CIMEL Sun photometer and the data are reported to the AERONET data base [*Holben et al.*, 1998]. The technical details of the instrument are described in the CIMEL Sun Photometer Manual (http://aeronet.gsfc.nasa.gov). The values of AOT presented in this work were selected at the quality level 2.

[11] The Aerosol Index (AI) data obtained from Ozone Monitoring Instrument (OMI) were used to describe the dust outbreak [*Levelt et al.*, 2000]. The AI concept, which was

developed based on the Total Ozone Mapping Spectrometer (TOMS) observations in the near UV, was applied to the OMI measurements [*Veihlmann et al.*, 2007]. This index allows the detection of absorbing aerosols through the spectral difference between the 340 nm and 380 nm. It is positive for absorbing aerosol at UV wavelength, such as dust, and negative for non-absorbing aerosols, such as sulfates [*Herman et al.*, 1997; *Herman and Celarier*, 1997; *Torres et al.*, 1998, 2002]. Moreover, for clouds, the values of AI are near zero [*Hsu et al.*, 1999]. The AI values presented in this work were selected at the quality level 3 with resolution of $1^\circ \times 1^\circ$. The AI index has provided information about dust horizontal distribution over land and ocean surface in many studies [e.g., *Alpert et al.*, 2000; *Barkan et al.*, 2005; *Bobely-Kiss et al.*, 2004; *Chiapello and Moulin*, 2002; *Engelstaedter and Washington*, 2007; *Israelevich et al.*, 2002; *Prospero et al.*, 2002].

[12] The evolution of the precipitation accumulated during the study period can be seen in the TRMM product 3B-42 within $\pm 50^\circ$ latitudinal belt, with a grid spacing of 25 km. The TRMM product was obtained using the TRMM Online Visualization and Analysis System (TOVAS) developed at NASA [*Acker and Leptoukh*, 2007]; http://daac.gsfc.nasa.gov/techlab/giovanni). The TRMM product used in this work was selected at the quality level 3 [*Huffman et al.*, 2007].

2.2. Meso-NH Model

[13] The mesoscale, nonhydrostatic atmospheric model Meso-NH was used in this study. This model has been jointly developed by the Centre National de la Recherche Meteorologique (CNRM, Meteo France) and the Laboratoire d'Aérologie (LA, CNRS) [*Lafore et al.*, 1998]. The capability of Meso-NH to simulate dust emissions and transport has been highlighted in several recent studies [*Bou Karam et al.*, 2009; *Crumeyrolle et al.*, 2008; *Chaboureau et al.*, 2011; *Tulet et al.*, 2010]. Meso-NH contains different sets of parameterizations such as cloud microphysics [*Cohard and Pinty*, 2000], turbulence [*Bougeault and Lacarrere*, 1989], lightning processes [*Barthe et al.*, 2005], gas-phase chemistry [*Suhre et al.*, 1998], aerosol chemistry [*Tulet et al.*, 2005, 2006] and dust aerosol [*Grini et al.*, 2006]. Natural land surfaces are described by interactions treated in the Soil Biosphere and Atmospheric model (ISBA) [*Noihlan and Mahfouf*, 1996].

[14] Meso-NH uses the radiation code of the ECMWF [*Fouquart and Bonnel*, 1980; *Morcrette and Fouquart*, 1986] which computes the radiative fluxes of shortwave and longwave radiation. Clouds and aerosols in the shortwave are taking into account using the Delta Edington transformation [*Joseph et al.*, 1976].

2.2.1. Mineral Dust Parametrization

[15] The dust emission scheme is the Dust Entrainment And Deposition (DEAD) model [*Zender et al.*, 2003], implemented as a component of Meso-NH [*Grini et al.*, 2006] that calculates dust flux from wind friction speed. The physical basis of the model is taken from *Marticorena and Bergametti* [1995] in which dust fluxes are calculated as a function of saltation and sandblasting processes. The dust emissions are forced directly by the surface flux parameters of the land surface scheme, and then distributed into the atmosphere in a manner which is consistent with the vertical fluxes of momentum, energy and moisture. In this parameterization, the three lognormal dust modes are generated and transported by the ORganic Inorganic Log-normal Aerosols Model (ORILAM) aerosol scheme [*Tulet et al.*, 2005, 2006]. These modes are described by their 0th, 3rd and 6th moments. The initial dust size distribution contains three lognormal modes with median radii of 0.039, 0.32 and 2.5 μm and standard deviation of 1.75, 1.76 and 1.70 respectively [*Crumeyrolle et al.*, 2008]. The ORILAM model simulates transport and dry deposition of aerosol. The dry deposition and sedimentation of aerosol are driven by the Brownian diffusivity and the gravitational settling [*Tulet et al.*, 2005]. In this study, the 0th and 6th moment are kept constant, which implies that the dispersion and radius mean of each dust mode are kept constant during the simulation.

[16] Aerosol scavenging is determined according to a kinetic approach to calculate the aerosol mass transfer in cloud and rain droplets as defined by *Tost et al.* [2006]. The scavenging by raindrops depends mainly on Brownian motion, interception and inertial impaction described by *Slinn* [1979]. Thus, within this scavenging scheme, the collection efficiency is calculated for these three types of collection. In agreement with the work of *Slinn* [1979], the small particles (radius below 0.1 μm) are collected efficiently by raindrops and cloud droplets through Brownian diffusion, the larger particles (radius above 10 μm) through inertial impaction. Inside the cloud, impaction scavenging by cloud droplets is less efficient for particles with radii from 0.1 to 1.0 μm [*Slinn*, 1979]. The in-cloud mass aerosol transfer into rain droplets by autoconversion and accretion processes have been introduced as described by *Pinty and Jabouille* [1998]. The sedimentation of aerosol mass included in raindrops has been simulated using a time splitting technique with an upstream differencing scheme of the vertical sedimentation raindrop flux [*Tulet et al.*, 2010]. The release of aerosol into the air due to rain evaporation is assumed to be proportional to the evaporated water [*Chin et al.*, 2000]. Regarding the shortwave effect, a refractive index of the dust aerosol was assigned according to that measured during the African Monsoon Multidisciplinary Analysis (AMMA) campaign [*Mallet et al.*, 2009]. The dust refractive index was taken from *Tulet et al.* [2010]; $1.448–2.92\ 10^{-3}$i for wavelengths between 440 and 690 nm, and $1.440–1.16\ 10^{-3}$i for wavelengths between 690 and 1190 nm. These dust refractive indices were obtained using AERONET retrievals for five Saharan sites during the AMMA campaign.

2.2.2. Simulation Configuration

[17] The simulation started at 00 UTC on 25 May 2008 and ended at 00 UTC on 1 June 2008. The study domain that covers the EUCAARI campaign area and a large part of the northern Africa extends between 15.1°N and 68.7°N latitude and 14.9°W and 23.1°E longitude, with a grid spacing of 25 km. This domain allows a large scale view of the dust transport. The vertical grid spacing consists of 60 stretched vertical levels reaching an altitude of 30 km. Initialization and lateral boundary conditions of the domain are taken from ECMWF operational analysis. Deep and shallow convection parameterization [*Bechtold et al.*, 2001] based upon the *Kain and Fritsch* [1993] mass flux scheme

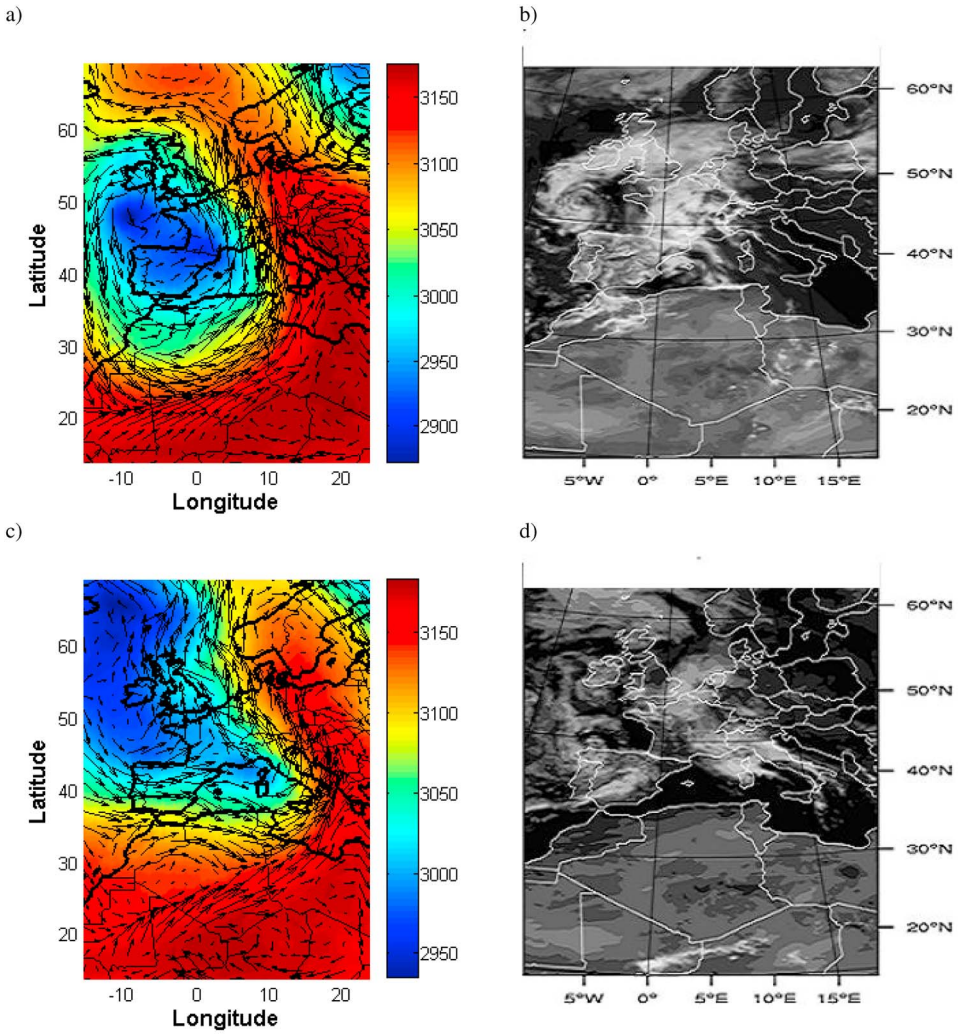

Figure 1. Synoptic situation on (top) 27 May and (bottom) 29 May 2008: (a and c) 700-hPa geopotential height (shading) and wind (vectors) at 1200 UTC from ECMWF analyses and (b and d) Meteosat Second Generation (MSG) images at 0.6 μm (at 1200 UTC 27 May (Figure 1b) and 1230 UTC 29 May (Figure 1d)).

is used for this study. Deep and shallow convective drafts horizontally exchange mass with their environment through detrainment of cloudy air and entrainment of cloud-free air. Subgrid-scale fluxes through convective updrafts and mixing with the environment through entrainment and detrainment are diagnosed in terms of grid-scale thermodynamic and dynamic variables [*Bechtold et al.*, 2000]. The implicit dust scavenging is parameterized following the mass flux calculated from the convection scheme aforementioned. The explicit dust scavenging is resolved by the wet deposition parameterization [*Tulet et al.*, 2010] where collection efficiency and kinetic mass transfer of aerosols into cloud droplets are computed by ICE3 microphysics scheme [*Pinty and Jabouille*, 1998].

[18] Three types of simulations were performed by taking into account only the dust. The reference simulation (REF) uses the implicit and explicit dust scavenging schemes in order to assess the dust transport toward northern Europe. Two other simulations were run to show the impact of precipitation on the dust distribution. The simulation SCAV used the implicit dust scavenging scheme whereas the NOSCAV simulation did not include any wet deposition.

3. Characteristics of the Saharan Dust Event

3.1. Meteorological Situation Over Europe

[19] The synoptic situation over Europe during the 16–31 May 2008 period was marked by strong convective activities associated to passage of a frontal system [*Hamburger et al.*, 2011]. The geopotential height and the wind flow at 700 hPa from ECMWF analysis is shown at 1200 UTC on 27 and 29 May 2008 (Figures 1a and 1c). The 700 hPa level was chosen because the average transportation of the dust takes place between the 600 and 800 hPa levels [*Hamonou et al.*, 1999; *Westphal et al.*, 1987]. On 27 May, a trough extended along the European and African coast while a high-pressure center was located over Italy (Figure 1a). Between the two systems, a steep gradient of pressure was observed resulting in a strong southwesterly flow from northern Africa toward the Mediterranean Sea. On 29 May, both the front and

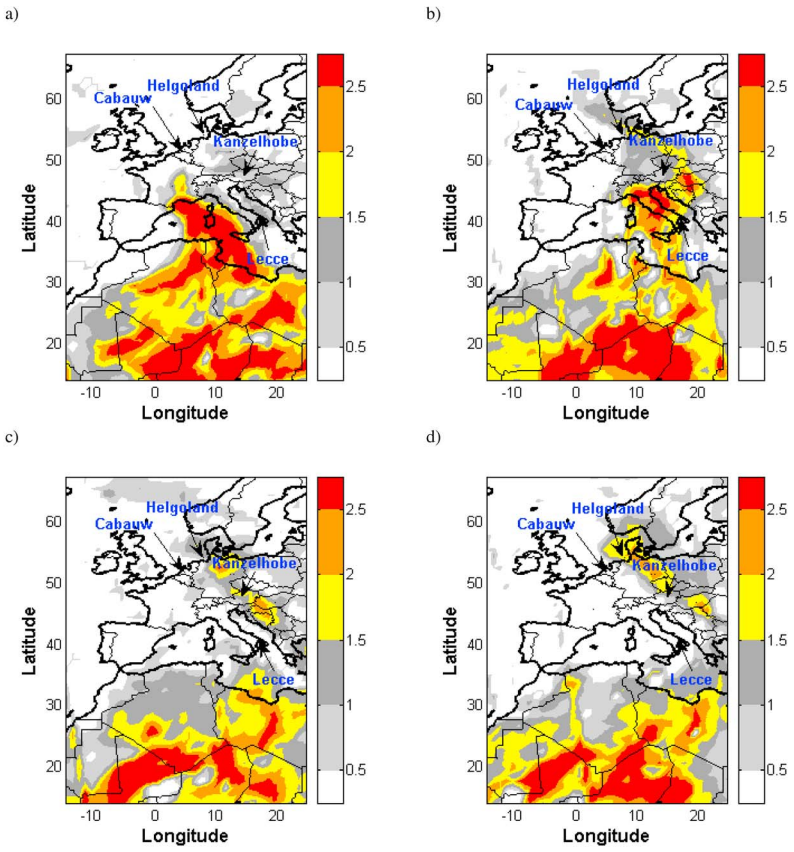

Figure 2. OMI aerosol index at 1200 UTC on (a) 27 May, (b) 28 May, (c) 29 May, and (d) 30 May 2008.

the high-pressure located over central Europe moved eastward (Figure 1c). These two synoptic systems produced a south-westerly flow in which the African air mass was embedded and transported toward the shores of the Baltic Sea.

[20] Meteosat Second Generation (MSG) images at 0.6 μm are shown on 27 May 2008 at 1200 UTC and 29 May 2008 at 1230 UTC (Figures 1b and 1d). On 27 May, a cyclonic rolling of clouds can be seen over the Atlantic Ocean near the northwestern coast of Spain as well as strong convective activity over southwestern France (Figure 1b). On 29 May, these convective clouds moved eastward over Italy (Figure 1d), where precipitation events greater than 45 mm per day were estimated by the Tropical Rainfall Measurement Mission (TRMM) product. Central Europe was mainly affected by heavy precipitations on that day (not shown).

3.2. Formation and Transport of an Intense Dust Plume Over Western Europe

[21] AI is a column integrated measure of the atmospheric dust content and therefore provides information about the horizontal distribution of the dust load. Figure 2 displays the evolution of the AI over the northern Africa and western Europe during our study. On 27 May 2008 at 1200 UTC (Figure 2a), dust was present over northern Africa (AI = 2.5) and nearby southeastern France (AI = 1). Over northern Africa, the largest values of AI were found between 15°N and 36°N, close to some well-identified sources of dust [*Caquineau et al.*, 2002; *Moulin et al.*, 1998; *Prospero et al.*, 2002]. Values greater than 2 were found over southern Tunisia, northern Algeria, northwestern Libya and the Bodélé depression near Lake Chad. A steep gradient between the low and the high pressure cells (Figure 1b) suggests the existence of a strong southeastern flow through which the Saharan dust was transported toward the Mediterranean Sea on 27 May 2008. On 28 May (Figure 2b), the dust spread to Italy and eastern Europe, with AI values greater than 1.5 over Germany and Hungary. A dust layer even reached northern Europe as shown by AI values around 2 over the shores of the Baltic Sea. On 29 May (Figure 2c), the dust coverage over the Mediterranean Sea was smaller certainly because of the strong convective activities. Moreover, it is worth noticing that the presence of dust plume over Italy was not observed because of the presence of clouds. In fact, the amount of aerosol detected in a cloudy region is reduced because clouds obscure of the aerosol layer. Low values of AI (less than 1) over the Mediterranean region correspond well with high values of rainfall as retrieved from the TRMM product. Therefore, it can be assumed that precipitation has probably scavenged the major part of dust over the Mediterranean region. In contrast, the dust coverage was greater over the shores of the Baltic Sea and over eastern Europe on 29 May. Within this area, the AI values ranged from 1 to 2.5 with maximum values observed over northeastern Germany and Hungary. On 30 May, the dust coverage continued its spread toward the north of Europe and extended from Hungary to Norway (Figure 2d).

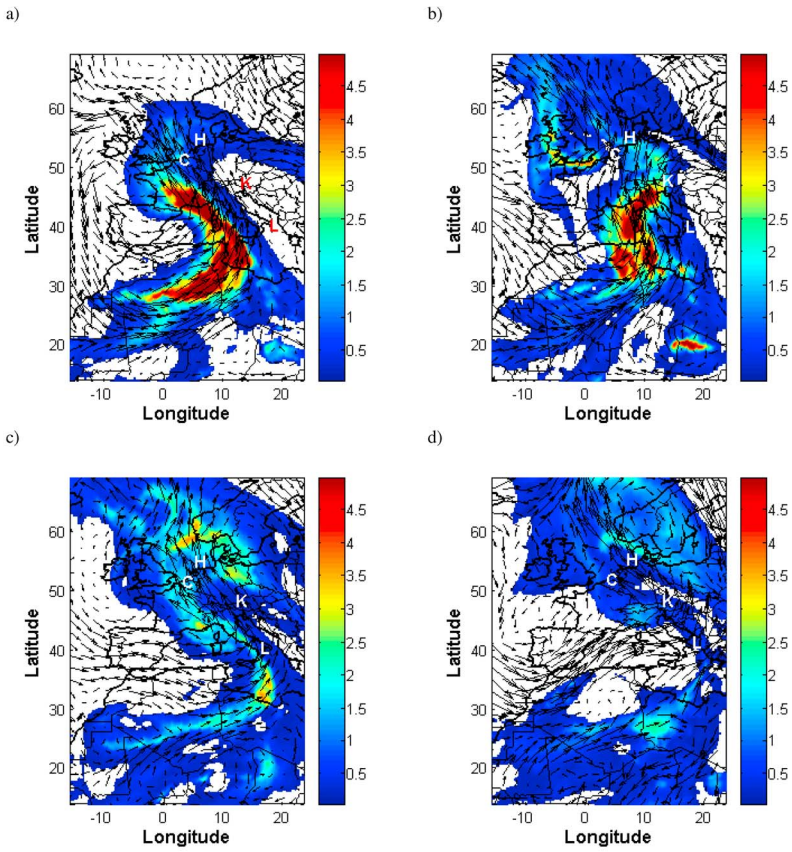

Figure 3. Aerosol optical thickness due to dust (shading) and 700 hPa wind (vectors) from the REF simulation at 1200 UTC on (a) 27 May, (b) 28 May, (c) 29 May, and (d) 30 May 2008. The locations of the Cabauw, Helgoland, Kanzelhohe and Lecce sites are represented by C, H, K and L, respectively.

3.3. AOT Evolution During the Dust Transport

[22] The evolution of the dust-AOT due to the presence of Saharan dust was simulated by Meso-NH in this large domain and shown in Figures 3a–3d. After 2 days of model integration, a belt of high dust-AOT extended in a large area from central Algeria to France passing by northeastern Libya (Figure 3a). Within this area the values exceed 4.5, particularly over central Algeria and northeastern Tunisia where values of 5.8 and 5.2 have been simulated, respectively. On 28 May, this belt of high dust-AOT extended from northeastern Libya to the northern Italy with values exceeding 4.5 (Figure 3b). An area of high dust-AOT (around 3) located over the English Channel has also been simulated. On 29 May, the belt of high AOT has disappeared, (Figure 3c). The simulated dust-AOT decreased by half within the Italian region (values did not exceed 2.5) whereas the dust-AOT increased over northern Europe. In particular, two high dust-AOT values (around 3) have been simulated around the Scandinavia region. On 30 May, the dust-AOT generally decreased within the domain, but there were significant peaks of 1.5 to 2 from Denmark to Sweden (Figure 3d). It is worth to note that the shape and the temporal distribution of the dust plume simulated by Meso-NH are similar to the shape and the temporal distribution observed by OMI, which implies that the dynamics conditions such as wind fields were well reproduced by Meso-NH (Figures 3a–3d).

[23] The observed AOTs have been compared to the simulated ones with the REF configuration (Figure 4). The Lecce station is located in the southeastern corner of Italy which is the closest station from the dust source zone. It is also the station located in the Mediterranean region which was less affected by precipitation. The observed AOT ranged from 0.18 to 0.51 with a maximum appeared on 30 May, indicating that Lecce was not very affected by the dust plume (Figure 4a); which we found also in the simulation. Based on Sun photometer measurements at Lecce, *Perrone et al.* [2005] found that the Saharan dust events over Lecce are generally characterized by AOT larger than 0.5. The observed AOT over Kanzelhohe ranged from 0.15 to 0.49 (Figure 4b). We note that the model simulated the passage of the dust plume over Kanzelhohe between 28 and 29 May, which is in agreement with the OMI observations previously shown (Figure 2). Unfortunately, AOT data were not recorded between 28 and 29 May owing to the presence of clouds. The Helgoland station is located in the vicinity of the German Bight, which is the farthest station from the dust source region. The observed AOT ranged from 0.1 to 0.8 (Figure 4c) with a median of 0.2. The maximum observed values occurred on 31 May. The simulated dust-AOT reveal the passage of the dust plume over Helgoland between 29 and 30 May.

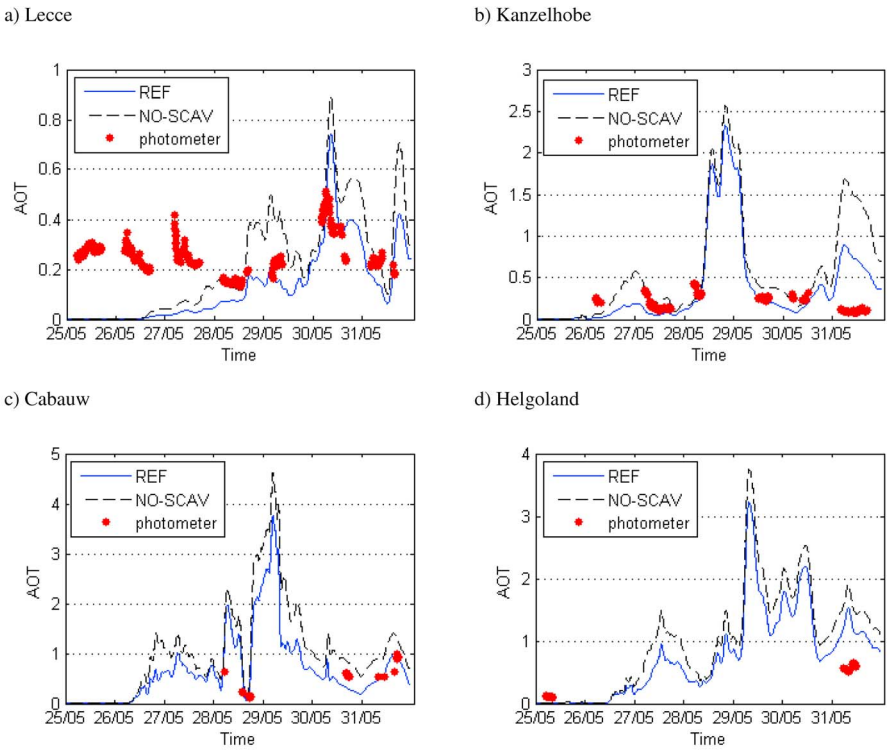

Figure 4. Aerosol optical thickness simulated at 440 nm (red dots) and calculated at 500 nm by REF (blue solid line) and NO-SCAV (black dashed line) simulations between 25 and 31 May 2008.

[24] Both the observations and the REF simulation show that the dust transport over northwestern Europe occurred in atmospheric conditions marked by strong convective activities. The discrepancies between Meso-NH and the observations can be attributed to several possible sources of forecast error. Thus, a possible sources of forecast error can be an underestimation of the precipitation (and wet scavenging) simulated by Meso-NH using a resolution of 25 km. Another possible explanation in these differences can come from the predictability of atmospheric model. Meso-NH is a forecasting atmospheric model. As such, it makes its own forecast and, as for all atmospheric models, a numerical drift can appear and increase as the simulation moves away from the initial conditions. Nevertheless, the simulated dust-AOT at Cabauw compared well with that observed (Figure 4d), and the AOT peak observed on 31 May with a maximum of 1 was well reproduced (the dust optical properties over the Netherlands will be discussed in more detail in Section 5). Overall, Meso-NH reproduced the dust transport toward northwestern Europe acceptably well and clearly indicated the Sahara as the dust source.

4. Quantitative Evaluation of the Dust Transport

4.1. Evaluation of the Net Flux

[25] It was clearly shown through the observations and the simulations that the Saharan dust was transported over northwestern Europe. The next step is to estimate the desert dust flux emitted and deposited by dry deposition during this period. Figure 5 depicts the spatial distribution of the net flux of dust accumulated at surface during the 25–31 May period. We define net flux as the difference between the dust amount emitted and that lost by dry deposition. Thus, a negative net flux corresponds with dust loss via dry deposition whereas a positive net flux corresponds with dust emission. The dust emission regions are only located in the northern Africa with values ranging from 0.04 to 0.25 kg m^{-2} (Figure 5). High positive net fluxes have been mainly simulated in southern Tunisia (0.25 kg m^{-2}), northeastern Algeria (0.22 kg m^{-2}), southwestern Morocco (0.2 kg m^{-2}) and northwestern Libya (0.2 kg m^{-2}). The most intense dust emission simulated in Tunisia and Algeria areawere close to

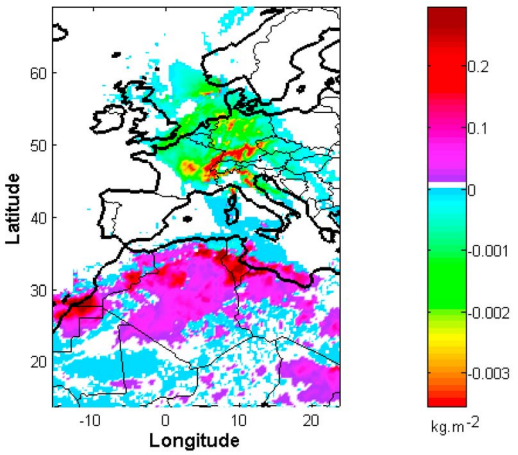

Figure 5. Net surface flux of dust (kg m^{-2}) from the REF simulation during the 25–31 May 2008 period.

Table 1. Estimates of Daily Dust Mass Emitted (in Tg) by Meso-NH Between 25 and 31 May 2008

	Days							
	05/25	05/26	05/27	05/28	05/29/	05/30	05/31	Total
Mass (Tg)	49	57	17	26	6	10	20	185

the "chott" regions. These extensive systems of salt lakes and dry lakes are known for their intense activity in April–May [*Prospero et al.*, 2002]. Thus, the dust emission regions simulated are consistent with the most significant, well-identified sources of dust in North Africa [*Engelstaedter et al.*, 2006; *Koren et al.*, 2003; *Mahowald et al.*, 2003]. For this episode, the origin of the dust transport across the Mediterranean and Europe is mainly from the North African dust sources (i.e., Tunisia, Algeria and Libya).

[26] From the simulated net flux, the mass budget of dust was estimated. Table 1 reports the daily amount of dust mass emitted between 25 and 31 May 2008. The estimates of the dust mass emitted are based on the sum of emissions from the individual source regions. They ranged from 6 to 57 Tg, with a maximum on 26 May and a minimum on 29 May. The total amount of emitted dust was estimated to be 185 Tg. Given the annual dust emission from North Africa of 1400 $Tg.yr^{-1}$ [*Ginoux et al.*, 2004], this dust episode represents 13 % of the annual emission. The estimates of dust loss by dry deposition are reported in Table 2. The amount of dust lost by dry deposition ranged from 0.5 to 3.0 Tg, with a maximum on 27 May and a minimum on 30 May. It is interesting to note that the dust loss by dry deposition has not been only simulated over Europe, but also over northern Africa and the Mediterranean basin. The total amount of dust lost by dry deposition was estimated to 12.5 Tg, which represents only 7 % of the total dust emission. Note that the dust amounts lost by dry deposition were more important in northern Africa (9.8 Tg) than in Europe (2.7 Tg). According to the meteorological situation described in Section 3.1, we cannot exclude a significant contribution of the wet deposition since Saharan dust is often deposited in precipitation over Europe [*Goudie and Middelton*, 2001]. In the following subsection, the contribution to the wet deposition will be described in more detail.

4.2. Dust Scavenging

[27] The impact of precipitation on dust size distribution is evaluated using Meso-NH through the realization of three simulations: the reference simulation (REF) that integrates the implicit and explicit dust scavenging scheme, the SCAV simulation which integrates only the implicit scheme and the NOSCAV simulation without wet deposition. The evolution of the explicit and implicit accumulated precipitations obtained from REF on 29 and 30 May is shown in Figures 6b and 6d, respectively. The evolution of the precipitation accumulated during the period aforementioned can be seen in the TRMM product 3B-42 (Figures 6a and 6c). There is a fairly good agreement between the Meso-NH simulation and the satellite observations during these two days. This is particularly true on 30 May (Figures 6c and 6d), when the strong convective activities ended over the Mediterranean basin. With the exception of northeastern Switzerland, precipitation was overestimated by Meso-NH. Indeed, within this region precipitation of 35 mm was simulated by Meso-NH whereas precipitation of 15 mm was observed by TRMM. Thus, within the northeastern Switzerland region the overestimation of the precipitation by Meso-NH reach a factor 2.3. However, on 29 May (Figures 6a and 6b), precipitation was underpredicted over the Mediterranean basin. It is worth to note that the intensity of the precipitation observed over the north Italian region (45 mm) was well reproduced by Meso-NH (Figures 6a and 6b). Overall, the precipitation associated with the passage of a frontal system over Mediterranean basin was reproduced by Meso-NH fairly well.

[28] From the dust burden modeled for the three simulations, we obtained an estimate of the dust mass scavenged over the European part of the study domain. Implicit precipitations decrease the dust mass from 93 Tg to 36 Tg, whereas explicit precipitations decrease the dust mass from 93 Tg to 75 Tg. Thus, 57 Tg were removed by implicit scavenging whereas 18 Tg were deposited by explicit scavenging. As a conclusion, dust was mainly removed by implicit precipitation. However, the impact of the explicit precipitation was not negligible even with a subgrid resolution of 25 km. The difference in dust-AOT evolution between the REF simulation and the NOSCAV simulation is shown in Figure 4. As expected, dust-AOTs from the NOSCAV simulation (without any dust scavenging) were higher than those from the REF simulation. AOTs in the NOSCAV simulation were about 1.5 times higher than the REF simulation. The maximum of difference between the two simulations is found at Lecce and Kanzelhohe and is consistent with greater amounts of precipitation observed by TRMM in central Europe compared to northern Europe.

5. Passage of the Dust Plume Over the Netherlands

5.1. Optical Properties of the Dust Plume

[29] The presence of dust over some regions of the northern France and the Netherlands was not observed by satellite because of the presence of clouds. However, the ground based measurements provide information about the optical properties of the dust plume over Cabauw. From the UV lidar observations at 353 nm, the vertical structure of clouds and aerosols can be assessed over Cabauw during the 27–30 May period. The presence of dust in the atmosphere can be observed by lidar, either via the aerosol extinction [*Hamonou et al.*, 1999; *Matthias et al.*, 2004; *Mattis et al.*, 2002] or the backscatter vertical profile [*Gobbi et al.*, 2000; *Mona et al.*, 2006]. Figure 7 depicts the evolution of

Table 2. Estimates of Daily Dust Mass Lost by Dry Deposition by Meson-NH Over Northern Africa and Europe Between 25 and 31 May 2008

	Days							
	05/25	05/26	05/27	05/28	05/29/	05/30	05/31	Total
Northern Africa (Tg)	1.3	2.7	2.4	1.1	1.0	0.4	0.9	9.8
Europe (Tg)	0.1	0.2	0.6	0.8	0.6	0.1	0.3	2.7

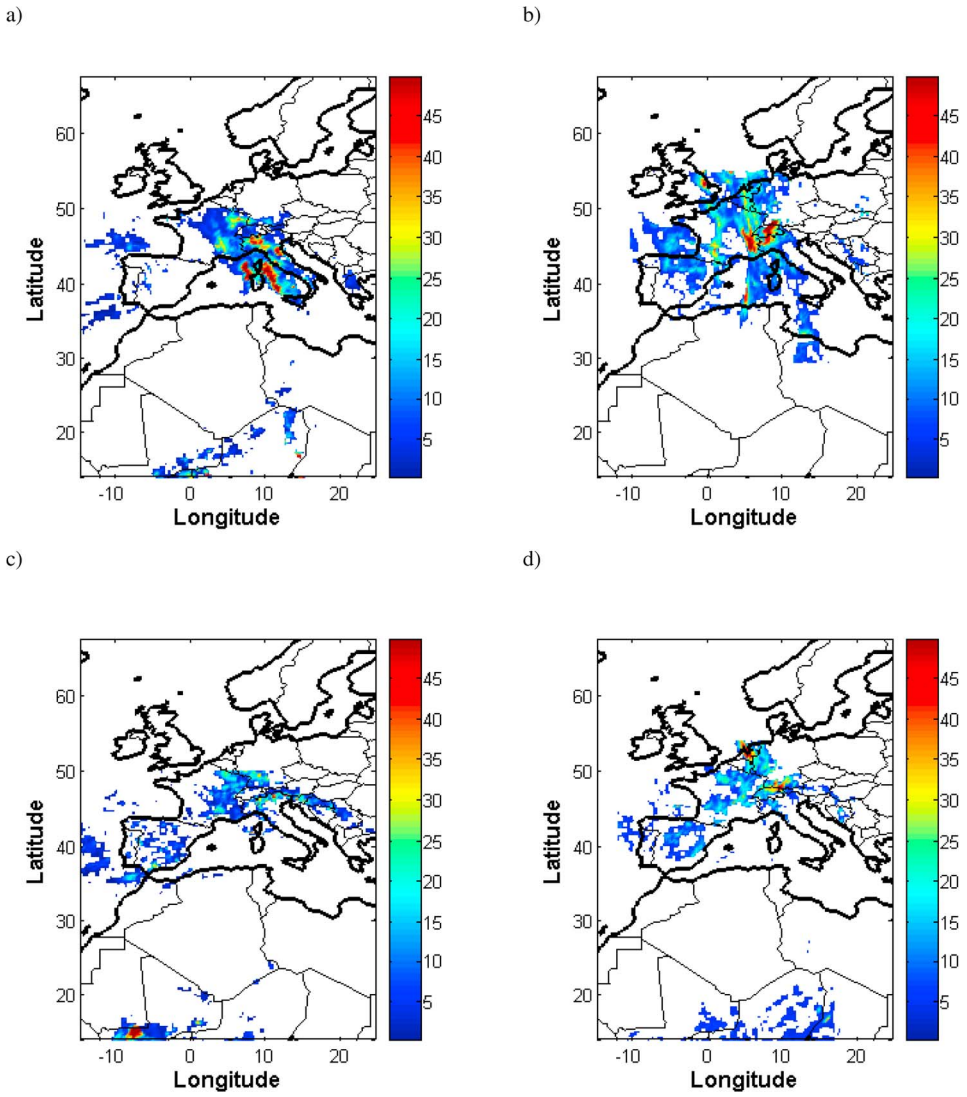

Figure 6. The 24-h accumulated precipitation (mm) from (a and c) the TRMM product 3B-42 and (b and d) the REF simulation valid at 00 UTC on (top) 29 May and (bottom) 30 May 2008.

the backscatter coefficient. As shown using MSG image at 0.6 μm (Figures 1b and 1d), observed backscatter coefficient larger than 5.10^{-3} km^{-1} sr^{-1} are due to clouds. Cloud layers in the lidar profile can easily be identified by the strong backscatter and the more inhomogeneous structure compared to aerosol layers [*Matthias et al.*, 2004]. Cabauw was affected by the presence of midlevel clouds (Figure 7), and particularly during the 28–29 May period. Moreover, the presence of aerosols inside the Planetary Boundary Layer (PBL) was characterized by backscatter coefficients around 3.10^{-3} km^{-1} sr^{-1}. As already discussed, *Hamburger et al.* [2011] showed that the synoptic situation during the first half of May 2008 has led to accumulation of aerosol inside the PBL, and particularly for the regions of northern Europe. Furthermore, they found that the maximum aerosol concentration was observed within the PBL above Cabauw.

[30] The observed backscatter coefficients ranged from 5 10^{-4} to 2 10^{-3} km^{-1} sr^{-1} are due to the Saharan plumes. We evaluated the thickness of the dust layer following the gradient method [*Mattis et al.*, 2008; *Mona et al.*, 2006; *Papayannis et al.*, 2008]. The base of the dust layer corresponds to the lowest point of a strong increase in the aerosol backscatter profile while the top of the dust layer is located at an altitude at which its first derivative become zero. The evolution of the thickness of the dust layer is shown on Figure 7 (in brown line). The thickness of the dust layer decreased slowly to 3.4 km on 28 May night, and slowly increased afterward up to 3.9 km on 29 May, and finally slowly decreased afterward down to 3.2 km on 30 May. The same behavior was observed for the top of the dust layer whereas the base generally was relatively constant during the observation period. On average, the base and the top of the dust layer was located at 0.9 and 4.5 km above sea level (asl), respectively.

[31] Figure 8 presents the evolution of the total (particle and gas) depolarization ratio at 353 nm during the 27–30 May 2008 period over Cabauw. The depolarization ratio ranged from 0.2 to 0.3 at 355 nm and can be used to identify desert

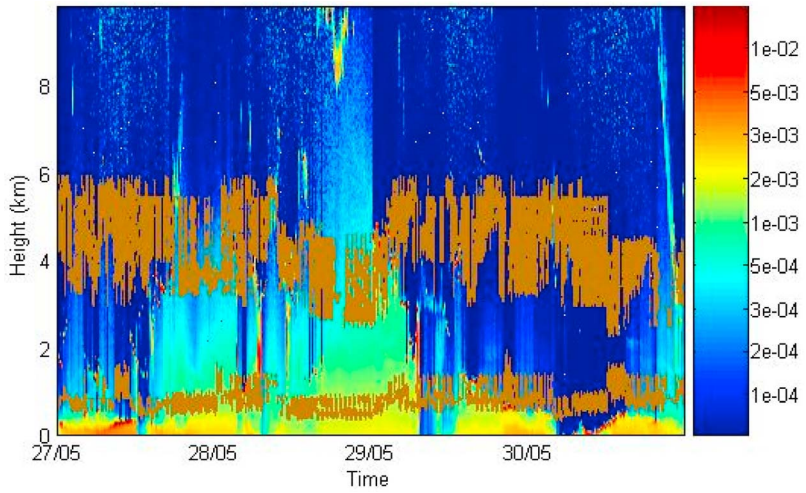

Figure 7. Time series of lidar backscatter coefficient (km^{-1} sr^{-1}) at 353 nm over Cabauw between 27 and 30 May 2008. The brown lines indicate the dust layer (bottom, top).

dust layers [*Gobbi et al.*, 2000; *Papayannis et al.*, 2008]. A particle depolarization ratio of 0.2–0.3 was found between 2 and 3.3 km asl, during the night of 27 May, indicating a dust layer (Figure 8). The depolarization ratio values ranged between 0 and 0.2, situated between 0.5 and 1.8 km asl, indicate a mixture of anthropogenic and dust particles [*Papayannis et al.*, 2008]. On 29 May morning, the dust particles were found near the surface. It is worth noticing that the presence of dust layer was masked by clouds with the depolarization ratio above 0.60. As a consequence, the dust layer seems to disappear sometimes on Figure 8, particularly on 29. Nevertheless, the depolarization ratios (Figure 8) confirm the presence of Saharan dust over the Netherlands, and the possibility of mixing processes of the dust with local aerosols.

[32] Figure 9 shows the temporal evolution of the AOT at 440 nm and the Angström exponent within the 440–870 nm wavelength range obtained from Sun photometer measurements at Cabauw between 28 and 31 May 2008. No data was recorded on 29 May due to the presence of clouds. As depicted in Figure 9, the AOT was under 0.4 only during the 28 May afternoon; otherwise, the AOT ranged from 0.5 to 1 with a maximum on 31 May. This is about 2-times higher than the average (0.29) and median (0.25) values usually measured at Cabauw [*Schaap et al.*, 2009], which corroborates the presence of aerosol during the dust episode.

[33] In spite of the presence of Saharan dust, the values of the Angström exponent differ from the values usually measured in presence of dust. As depicted by Figure 9, the Angström exponent ranged from 0.5 to 1.5, which is higher than the values usually observed in presence of Saharan dust [e.g., *Ansmann et al.*, 2003, 2011; *Collaud Coen et al.*, 2004; *Eck et al.*, 1999; *Hamonou et al.*, 1999; *Müller et al.*, 2003]. The Angström exponent is generally below 0.5 for large dust

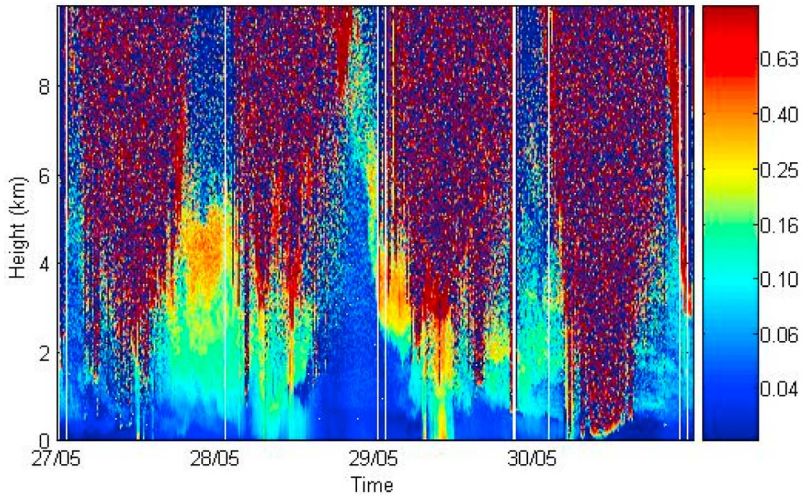

Figure 8. Time series of total depolarization ratio at 353 nm obtained from UV lidar at Cabauw (51.97°N, 4.93°E) between 27 and 30 May 2008. We note that the cloud screening process was not applied on this data. As a consequence, sometimes the presence of the dust layer was masked by clouds with the depolarization ratio above 0.60.

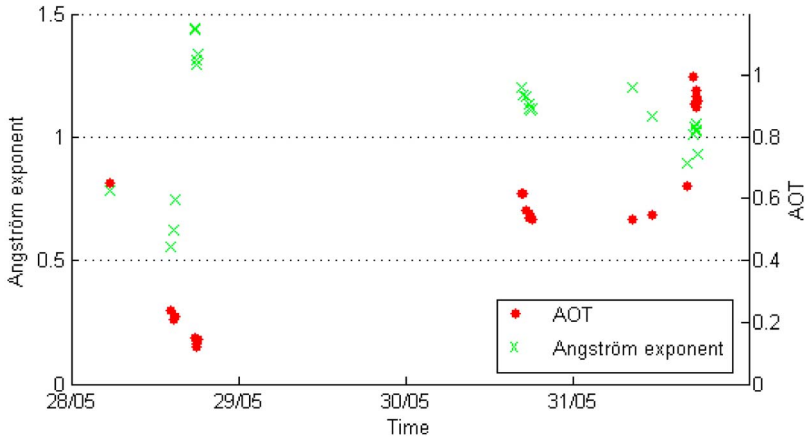

Figure 9. Aerosol optical thickness observed at 440 nm (red dots) and Angström coefficient calculated within the 440–870 nm wavelength range (green crosses) at Cabauw between 28 and 31 May 2008.

particles whereas it is above 1 for anthropogenic particles [*Ansmann et al.*, 2003]. The values of Angström exponents in this study suggest the predominance of small particles. Based on the meteorological situation (described in subsection 3.1), the high values of the Angström exponent found at Cabauw are a result of effective scavenging of the coarse mode during the Saharan dust transport over Europe. In certain cases, the dust "signature" is reduced when the dust is mixing with anthropogenic particles [*Balis et al.*, 2004].

[34] As previously mentioned (subsection 3.3), the simulated dust-AOT at Cabauw compared well with that observed (Figure 4d). Since the AOT is the vertical integral of the aerosol extinction coefficient over the whole atmosphere, we use an analysis of the scattering and extinction coefficient to better understand the physical properties of the dust over the Netherlands. The scattering coefficient obtained from the nephelometer on board the ATR-42 aircraft on 30 May from 1350 UTC to 1405 UTC is shown in Figure 10 (solid line). It was measured over a domain between 51.97°N and 51.88°N latitude and 6.05°E and 4.99°E longitude and at three wavelengths, at 450, 550 and 700 nm. The values ranged from 0.01 to 0.08 km^{-1} between 0.6 and 2.6 km asl. The scattering coefficient increased and reached its maximum values (0.05–0.08 km^{-1}) between 1.8 and 2.5 km asl from 1350 UTC to 1355 UTC, and quickly decreased afterward to 0.01 km^{-1} at 0.6 km asl. The scattering coefficient strongly decreases with the wavelength from 1350 UTC to 1355 UTC, which differs to that usually observed in presence of dust [*Collaud Coen et al.*, 2004]. This spectral dependence suggests some changes in particle physico-chemical properties and their size distributions [*Israelevich et al.*, 2003]. Because the fine mode generally shows a more pronounced wavelength dependence than the coarse mode [*Collaud Coen et al.*, 2004], the quantity of small particles (radius below 0.1 μm) has a larger effect than the number of large particles (radius above 10 μm). Furthermore, the spectral dependence of the scattering coefficient can be also determined by shape and the chemical composition (real and imaginary refractive indices) [*Ackermann*, 1998].

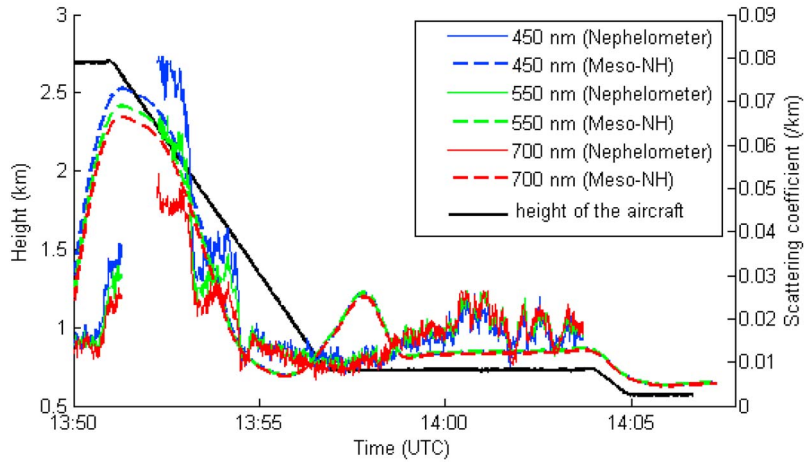

Figure 10. Scattering coefficient measured by the nephelometer (solid line) and simulated (dashed line) by REF around Cabauw between 1350 and 1410 UTC on 30 May 2008. The black line indicates the height of the aircraft.

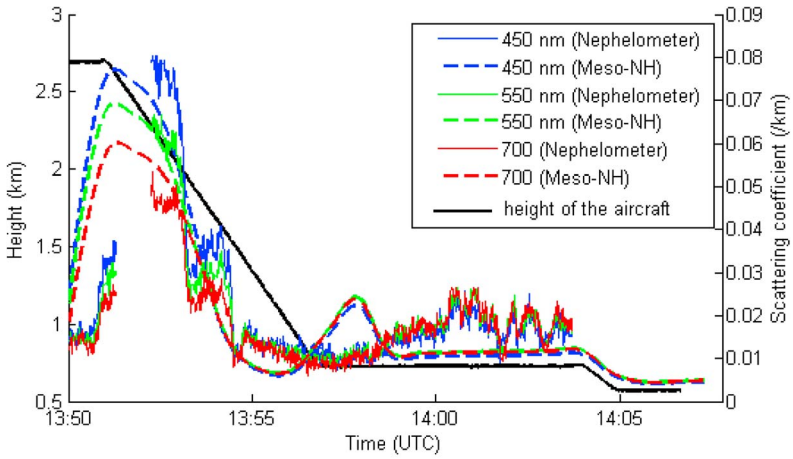

Figure 11. Scattering coefficient measured by the nephelometer (solid line) and simulated (dashed line) by REF with the new refractive indices around Cabauw between 1350 and 1410 UTC on 30 May 2008. The black line indicates the height of the aircraft.

[35] In order to better understand this strong spectral dependence, the airborne remote sensing measurements were simulated by Meso-NH (dashed line in Figure 10). The simulated scattering coefficient compared acceptably well with that observed. The maximum values (0.07 km^{-1}) at 450 nm were observed between 1350 UTC and 1355 UTC. The wavelength dependence of the scattering coefficient was much weaker in the model (Figure 10). This bias suggests that the aging of the dust therefore was not sufficiently taken into account by refractive indices determined during AMMA campaign [*Mallet et al.*, 2009; *Tulet et al.*, 2010]. In order to improve the simulation of the scattering coefficient over the Netherlands we have used others refractive indices. The values of the new refractive indices used are 1.470–3.99 10^{-3}i for wavelengths between 440 and 690 nm, and 1.453–1.32 10^{-3}i for wavelengths between 690 and 1190 nm. These new dust refractive indices were obtained using AERONET retrievals [*Dubovik et al.*, 2000; *Kim et al.*, 2011] for the Lecce site. It is worth to note that the values of the imaginary part of these new refractive indices are in agreement with the values determined during the SAMUM campaign [*Petzold et al.*, 2009]. The airborne remote sensing measurements were simulated by Meso-NH with these new refractive indices (dashed line in Figure 11). The new simulation of the scattering coefficient compared well with that observed (Figure 11). Furthermore, we note that the wavelength dependence of the scattering coefficient was well reproduced by Meso-NH by using these new refractive indices. Thus, the aging of the dust was sufficiently taken into account by these new refractive indices.

[36] The Single Scattering Albedo (SSA) at 550 nm obtained from the measurements of the nephelometer and the PSAP on board the ATR-42 aircraft on 30 May from 1350 UTC to 1405 UTC is shown in Figure 12a. The values ranged from 0.20 to 0.98 between 0.6 and2.6 km asl. The SSA increased and reached its maximum values (0.98) at 2.4 km asl from 1350 UTC to 1355 UTC, and quickly decreased afterward to 0.70 at 2 km asl. Between 0.6 and 1.5 km asl, the SSA quickly increased and stayed relatively constant to 0.90. The observed SSA between 0.6 and 2 km asl, indicate the presence of dust [*El-Metwally et al.*, 2008; *Kubilay et al.*, 2003; *McConnell et al.*, 2008]. Low values of SSA (0.2–0.4) were observed at 2.6 km asl, indicate the presence of very absorbing particles. The observed SSA have been compared to the simulated ones from REF (blue line in Figure 12a). The simulated SSA compared quite well with that observed. The simulated SSA ranged from 0.69 to 0.89, with the maximum simulated between 1355 UTC and 1405 UTC. The simulations were performed taking into account only the desert dust particles, which can cause biases in estimate of the SSA, particularly before 1355 UTC.

[37] The extinction coefficient at 550 nm obtained from the measurements of the nephelometer and the PSAP on board the ATR-42 aircraft on 30 May from 1350 UTC to 1405 UTC is shown in Figure 12b. The values ranged from 0.02 to 0.09 km^{-1} between 0.6 and 2.6 km asl. The extinction coefficient increased and reached its maximum values (0.09 km^{-1}) between 2.0 and 2.5 km asl from 1350 UTC to 1355 UTC, and quickly decreased afterward to 0.02 km^{-1} at 0.6 km asl. The observed extinction coefficients have been compared to the simulated ones from REF (blue line in Figure 12b). The simulated extinction coefficients compared quite well with that observed. The simulated extinction coefficients ranged from 0.01 to 0.08 km^{-1}, with the maximum simulated between 1350 UTC and 1355 UTC.

[38] To understand this vertical structure of atmospheric dust, a cross section of the extinction coefficient between the surface and 7 km asl at 1350 UTC on 30 May 2008 was made from REF simulation over the Netherlands (Figure 13). Two main dust layers were present and separated by a region of low values of extinction coefficient (less than 0.04 km^{-1}). These low values can be attributed to a scavenging of the dust inside this layer. The first dust layer was situated between 2.5 and 5.2 km high with the extinction maxima (0.09 km^{-1}) situated at 3.2 km asl. The second dust layer was located between 0.8 and 1.5 km asl which is separated in two parts by a region of low values (less than 0.03 km^{-1}). The first part of this second dust layer was located between (51.96°N, 5.78°E) and (51.91°N, 5.53°E) with the extinction maxima (0.08 km^{-1}) situated at 1 km asl. The second part of this second dust layer was located

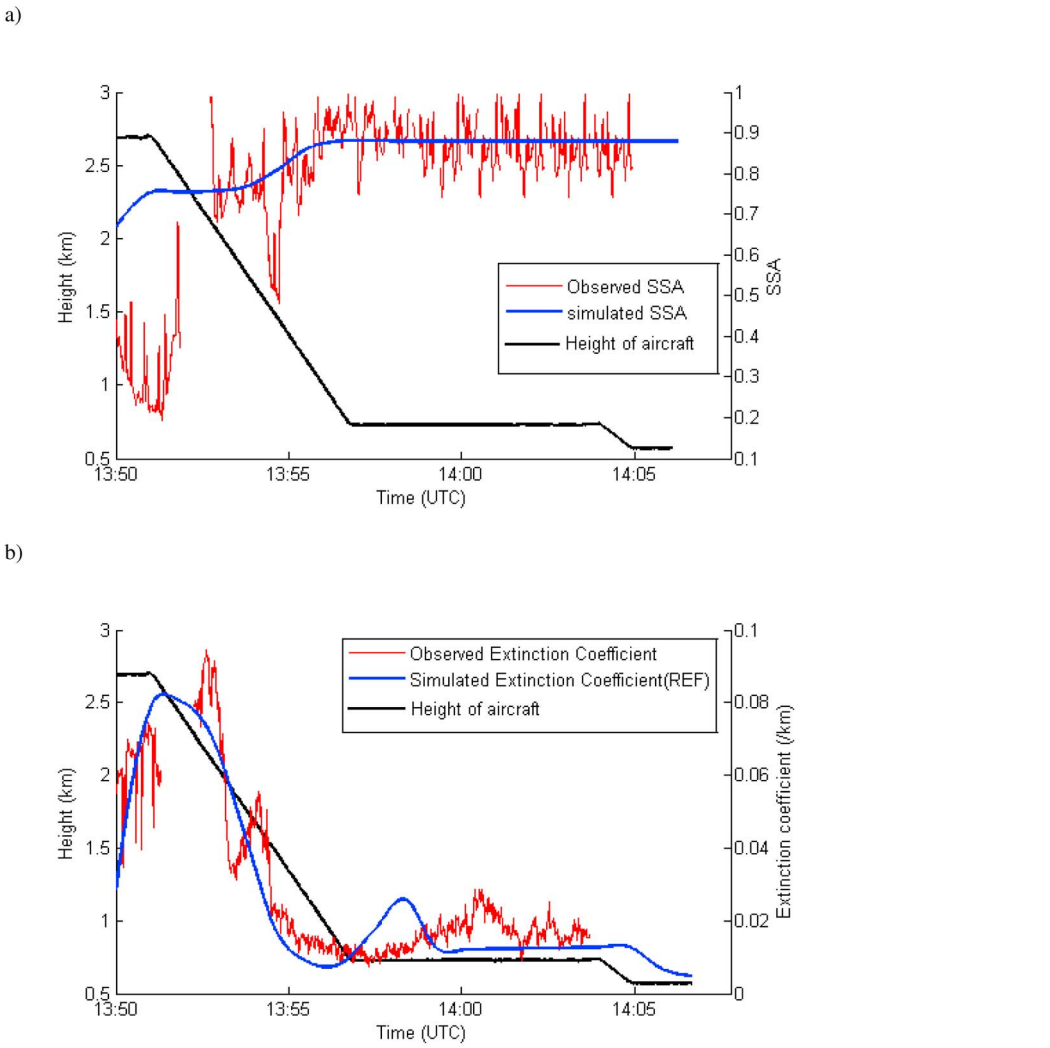

Figure 12. (a) SSA and (b) extinction coefficient simulated at 550 nm (blue line) by REF and observed at 550 nm (red line) around Cabauw between 1350 UTC and 1410 UTC on 30 May 2008 over the Netherlands between (51.96°N, 5.78°E) and (51.81°N, 5.06°E). The black line indicates the height of the aircraft.

between (51.85°N, 5.22°E) and (51.81°N, 5.06°E) with the extinction maxima (0.07 km^{-1}) situated at 1 km asl. Over some regions dust was found near the surface, with the extinction values of 0.06 km^{-1}, consistent with the lidar backscatter observations. These results suggest mixing processes between the dust and the anthropogenic sources of pollution over Cabauw, which may be generated locally or transported from far away. A strong extinction signal was observed when the aircraft passed through the lower part of the first dust layer situated at 2.5 km asl (dashed line in Figure 12). The contribution of the coarse and accumulation mode to extinction was analyzed over the same region from REF simulation (Figures 14a and 14b). The contribution of each mode is defined as the ratio between the extinction obtained for each mode and the total extinction. The results reveal that more than 80% of extinction above 2.5 km asl was due to the coarse mode (Figure 14a). Below 2.5 km asl, the extinction was mainly due to the accumulation mode (more than 70%), particularly between (51.96°N, 5.78°E) and (51.85°N, 5.22°E). Thus, the large peak of extinction coefficients (Figure 12b) was observed in a region where

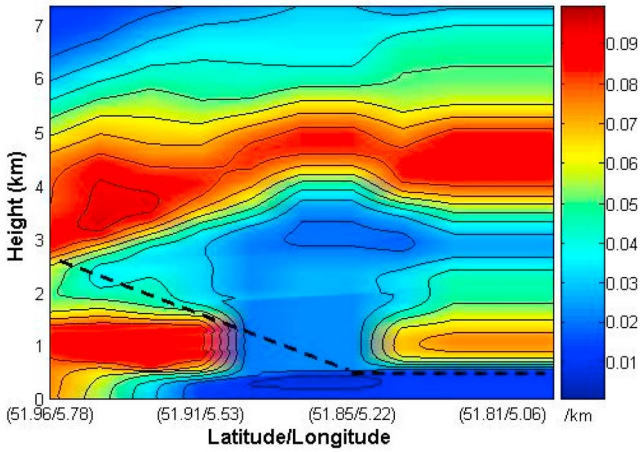

Figure 13. Vertical cross section of extinction coefficient at 1350 UTC on 30 May 2008 over the Netherlands between (51.96°N, 5.78°E) and (51.81°N, 5.06°E) calculated from REF simulation.

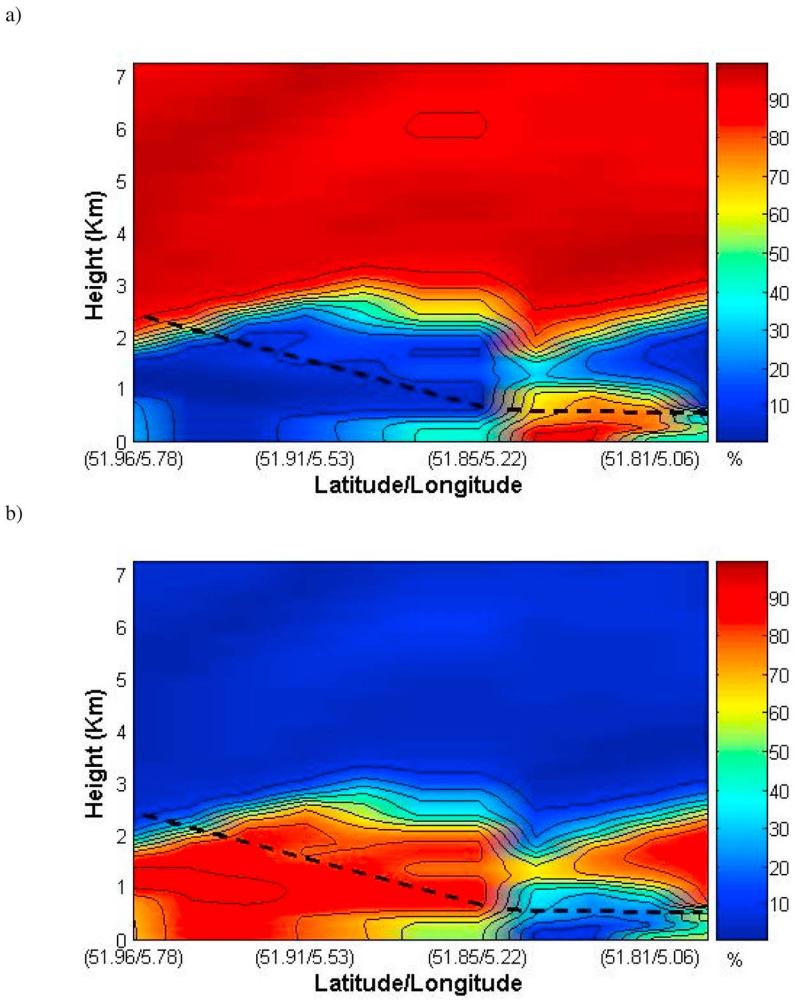

Figure 14. Contribution (in percentages) of the (a) coarse and (b) accumulation mode to extinction coefficient on 30 May 2008 over the Netherlands between (51.96°N, 5.78°E) and (51.81°N, 5.06°E) calculated from REF simulation.

80% of extinction was due to the accumulation mode (Figure 14b). It can be noticed that 75% of extinction below 1 km asl between (51.85°N, 5.22°E) and (51.81°N, 5.06°E) was due to coarse mode. The large difference in contributions of accumulation and coarse mode distributions suggests that the strong dependence on wavelength can be attributed to high precipitation scavenging efficiency for the coarse mode.

[39] *Balis et al.* [2004] shown that the mixing processes can induce a modification of the dust optical characteristics. Based on the black carbon mass concentration and cloud nuclei number concentrations for the European region in May 2008 [*Hamburger et al.*, 2011], mixing processes between the Saharan dust and anthropogenic particles likely occurred during their transport toward the Netherlands. Thus, we cannot ignore a possible influence of the mixing processes on the dust optical characteristics. Nevertheless, according to the meteorological situation and our results aforementioned, we are convinced that the evolution of dust optical characteristics observed over the Netherlands was mainly due to high precipitation scavenging efficiency for the coarse mode. In order to improve the discussion, the precipitation scavenging efficiency for each dust mode will be described in detail, in the following subsection.

5.2. Dust Vertical Distribution and Aerosol Size Filtering

[40] In order to better understand the dust size transported over the Netherlands, an analysis of the impact of the precipitation on dust size distribution is now presented. The profile of mass and number concentration for the three dust modes of Meso-NH are shown for the REF and NOSCAV simulations at Cabauw on 30 May at 1400 UTC (Figure 15a). The vertical profile of the accumulation mode with the median radius of 0.32 μm is the same for both the REF and NOSCAV simulations. In other words, this mode was not affected by impaction scavenging since these particles are too large to be collected by Brownian motion and too fine to be collected by inertial impaction. The collection efficiency factor was less than 10^{-3} for the accumulation mode whereas for the coarse mode (with median radius of 2.5 μm) the efficiency factor was close to 1 [*Tulet et al.*, 2010]. The differences between the profiles obtained from the REF and NOSCAV simulations for the fine dust mode

a)

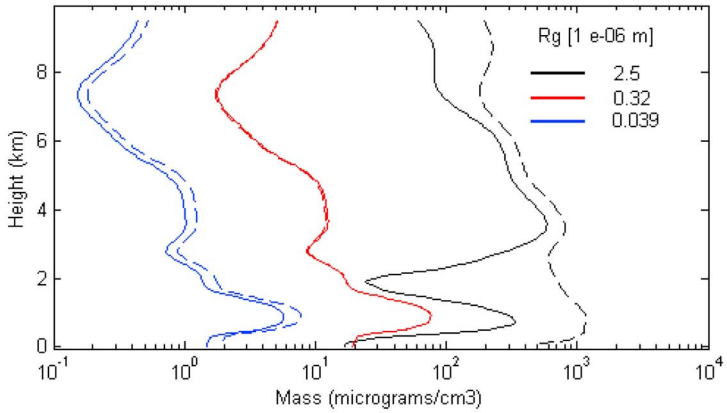

b)

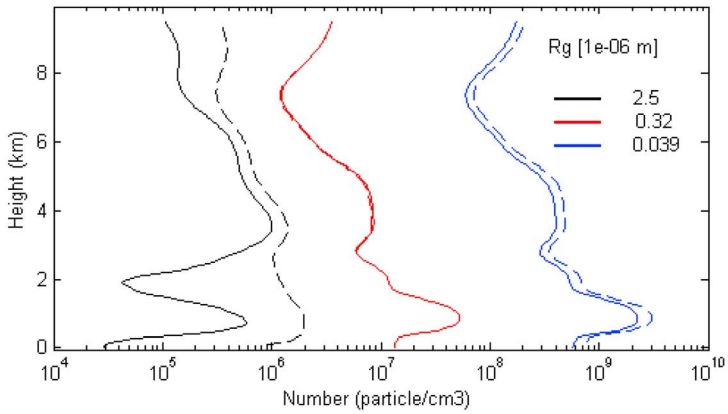

Figure 15. Vertical profile of (a) mass concentration (μg m^{-3}) and (b) particle concentration (m^{-3}) at Cabauw simulated by REF (with explicit and implicit scavenging, solid line) and NO-SCAV (dashed line) on 30 May 2008 at 1300 UTC. The concentrations were computed for modes at Rg = 0.039 μm (blue), Rg = 0.32 μm (red) and Rg = 2.5 μm (black).

(with the median radius of 0.039 μm) were small (losses are due to Brownian motion). As a consequence, the majority of the dust concentration of the larger mode was scavenged whereas the majority of the two smallest modes were preserved. The precipitation slightly decreases the dust mass concentration of the coarse mode above 4 km asl from 700 μg m^{-3} to 500 μg m^{-3}, whereas the decrease was much more significant below 4 km asl. The dust mass concentration reduced from 1100 to 380 μg m^{-3} close to the surface and from 600 to 50 μg m^{-3} at 2 km asl. Between the surface and 2.2 km asl the mass concentration of the coarse mode was similar to the one of the accumulation mode as the coarse mode was the most affected by the precipitation. This scavenging represents 85% of the total mass dust concentration. The number concentration of the two smallest modes was higher than the coarse mode (5.0 10^7 and 2.0 10^9 particles per m^3 at 1 km for the accumulation and fine mode, respectively, compared to 5.5 10^5 particles per m^3 of the coarse mode), as depicted by Figure 15b. The height interval where the dust coarse mode was significantly scavenged coincided with the strong wavelength dependence of the scattering coefficient and demonstrates that the high values of the Angström exponent are a result of strong scavenging of the dust coarse mode.

6. Summary and Conclusion

[41] The long-range dust transport over northwestern Europe during the EUCAARI intensive observational period, between 25 and 31 May 2008 was examined. The analysis focuses on the site of Cabauw, which was selected to quantify the regional aerosol properties, aerosol formation, transformation, transport and deposition during the EUCAARI 2008 campaign. The transport of dust to northwestern Europe was investigated by combining satellite, airborne and ground-based observations, and numerical experiments through the use of the non-hydrostatic meso-scale model Meso-NH. The synoptic situation in the second half of May 2008 over Europe was marked by strong convective activities associated to the passage of a frontal system over central Europe. The high-pressure system located over northern Africa moved slowly northward and favored the

spread of dust over northwestern and central parts of Europe while convection triggered ahead of the trough over western Europe. The AOT typically ranged from 0.1 to 0.5 at the wavelength of 440 nm, with maximum values close to 1 found over Cabauw. Through the use of the OMI-AI, it was well-identified that the dust coming from the western and central Sahara reached the northern Europe. The Meso-NH simulations were in fairly good agreement with the network observations. In particular over Cabauw, where the AOT peak observed on 31 May with a maximum of 1 was well reproduced. A dust episode was simulated on 29 May over Europe, however, this episode was not observed by AERONET due to the presence of clouds. The total amount of dust emitted during the study period was estimated to 185 Tg. The analysis of the removal processes revealed that only 7% of the total dust emitted was lost by dry deposition. Moreover, it was shown that the dust was mainly removed by implicit precipitation, but the impact of the explicit precipitation was not negligible in spite of a horizontal grid spacing of 25 km. In total, the amounts scavenging by implicit and explicit precipitations were estimated to 57 Tg and 18 Tg, respectively.

[42] From the UV lidar observations at 353 nm at Cabauw, the vertical structure of aerosol was assessed. The main dust layer was located between 2.5 and 5.2 km height, and the presence of dust was probed at 0.9 km asl. Values of the depolarization ratio indicated mixture of anthropogenic and dust particles between 0.5 km asl and 1.8 km asl on 29 May onwards. This suggests the possibility of dust to be mixed with anthropogenic emissions in Europe. Moreover we note that the depolarization ratio indicated possible mixing of dust haze. Airborne measurements embedded on the ATR-42 aircraft revealed a dependence of the scattering coefficient to the wavelength while the Angström exponent mainly ranged from 0.5 to 1.4 at Cabauw and its vicinity. As a result of the simulated transport and wet deposition of dust, aerosol impaction scavenging is shown to be the main process by which particles were deposited. This was due to high collection efficiency for the coarse mode, particularly below 4 km asl. It was also known that dust aerosols in clouds can act as ice nuclei [*Chou et al.*, 2011; *DeMott et al.*, 2003; *Seifert et al.*, 2010]. Furthermore, the dust particles can enhance their hygroscopic properties, by coating or adsorbing soluble materials during their transport, and favored the formation of cloud condensation nuclei [*Levin et al.*, 1996; *Sassen*, 2002; *Sassen et al.*, 2003; *Sullivan et al.*, 2009]. Further analysis of the dust microphysical properties such as dust mixing with anthropogenic aerosol will be examined in a forthcoming study.

[43] **Acknowledgments.** This work has been partially funded by European Commission 6th Framework program project EUCAARI and by the French National Research Agency (ANR) under the AEROCLOUD program. This work was financially supported by La Région Réunion and l'Europe. We thank Alfons Schwarzenboeck and the LAMP for the PSAP measurements. MSG observations were obtained from SATMOS through the ICARE Data and Service Center. Simulations were performed on the CNRS/IDRIS computers. The TRMM and OMI observations used in this paper were produced with the GIOVANNI online data system, developed and maintained by the NASA GES DISC. We thank M. R. Perrone, E. Putz, G. Leeuwe and R. Doerffer and their staff for establishing and maintaining the Lecce, Kanzelhohe, Cabauw and Helgoland sites used in this investigation. The authors especially want to thank the staff members of the team working on the airborne measurements aboard the ATR-42 during the EUCAARI campaign. We would like to acknowledge CESAR for the LIDAR data. We would like to thank the Meso-NH assistance team for their help and availability. We also would like to thank the CCUR team for the use of the TITAN supercomputer. During the submission of the initial draft, Laurent Gomes passed away. We dedicate this paper to the memory of a colleague and friend.

References

Acker, J., and G. Leptoukh (2007), Online analysis enhances use of NASA Earth science data, *Eos Trans. AGU*, *88*, 14–17, doi:10.1029/2007EO020003.

Ackermann, J. (1998), The extinction-to-backscatter ratio of tropospheric aerosol: A numerical study, *J. Atmos. Oceanic Technol.*, *15*, 1044–1050.

Alpert, P., J. Herman, Y. Kauffman, and I. Carmona (2000), Response of the climatic temperature to dust forcing, inferred from Total Ozone Mapping Spectrometer (TOMS) aerosol index and NASA assimilation model, *Atmos. Res.*, *53*(1–3), 3–14.

Anderson, T. L., and J. Ogren (1998), Determining aerosol radiative properties using the TSI 3563 integrating nephelometer, *Aerosol Sci. Technol.*, *29*, 57–69.

Anderson, T. L., et al. (1996), Performance characteristics of a high-sensitivity, three-wavelength, total scatter/backscatter nephelometer, *J. Atmos. Oceanic Technol.*, *13*, 967–986.

Ansmann, A., et al. (2003), Long-range transport to Saharan dust to northern Europe: The 11–16 October 2001 outbreak observed with EARLINET, *J. Geophys. Res.*, *108*(D24), 4783, doi:10.1029/2003JD003757.

Ansmann, A., A. Petzold, K. Kandler, I. Tegen, M. Wendisch, D. Müller, B. Weinzierl, T. Müller, and J. Heintzenberg (2011), Saharan Mineral Dust Experiments SAMUM-1 and SAMUM-2: What have we learned?, *Tellus, Ser. B*, *63*, 403–429.

Balis, D., V. Amiridis, S. Nickovic, A. Papayannis, and C. Zerefos (2004), Optical properties of Saharan dust layers as detected by Raman lidar at Thessaloniki, Greece, *Geophys. Res. Lett.*, *31*, L13104, doi:10.1029/2004GL019881.

Barkan, J., H. Kutiel, P. Alpert, and P. Kishcha (2004), The synoptic of dust intrusion days from the African continent into the Atlantic Ocean, *J. Geophys. Res.*, *109*, D08201, doi:10.1029/2003JD004416.

Barkan, J., P. Alpert, H. Kutiel, and P. Kishcha (2005), Synoptics of dust transportation days from Africa toward Italy and central Europe, *J. Geophys. Res.*, *110*, D07208, doi:10.1029/2004JD005222.

Barthe, C., G. Molinié, and J. Pinty (2005), Description and first results of an explicit electrical scheme in a 3D cloud resolving model, *Atmos. Res.*, *76*(1–4), 95–113.

Bechtold, P., et al. (2000), A GCSS intercomparison for a tropical squall line observed during TOGA-COARE. II: Intercomparison of single-column models and a cloud-resolving model, *Q. J. R. Meteorol. Soc.*, *126*, 865–888.

Bechtold, P., E. Bazile, F. Guichard, P. Mascart, and E. Richard (2001), A mass-flux convection scheme for regional and global models, *Q. J. R. Meteorol. Soc.*, *127*, 869–886.

Bobely-Kiss, I., A. Kiss, E. Koltay, G. Szabo, and L. Bozo (2004), Saharan dust episodes in Hungarian aerosol: Elemental signatures and transport trajectories, *J. Aerosol Sci.*, *35*(10), 1205–1224.

Bougeault, P., and P. Lacarrere (1989), Parametrization of orography-induced turbulence in a meso-beta model, *Mon. Weather Rev.*, *117*, 1872–1890.

Bou Karam, D., C. Flamant, P. Tulet, M. Todd, J. Pelon, and E. William (2009), Dry cyclogenesis and dust mobilization in the intertropical discontinuity of the West Africa Monsoon: A case study, *J. Geophys. Res.*, *114*, D05115, doi:10.1029/2008JD010952.

Caquineau, S., A. Gaudichet, L. Gomes, and M. Legrand (2002), Mineralogy of Saharan dust transported over northwestern tropical Atlantic Ocean in relation to source, *J. Geophys. Res.*, *107*(D15), 4251, doi:10.1029/2000JD000247.

Chaboureau, J., E. Richard, J. Pinty, C. Flamant, P. D. Girolamo, C. Kiemle, A. Behrendt, H. Chepfer, M. Chiriaco, and V. Wulfmeyer (2011), Long-range transport of Saharan dust and its radiative impact on precipitation forecast over western Europe: A case study during the Convective and Orographically induced Precipitation Study (COPS), *Q. J. R. Meteorol. Soc.*, *137*, 236–251.

Chiapello, I., and C. Moulin (2002), TOMS and METEOSAT satellite record of the variability of Saharan dust transport over the Atlantic during the last two decades (1979–1997), *Geophys. Res. Lett.*, *29*(8), 1176, doi:10.1029/2001GL013767.

Chin, M., R. Rood, S. Lin, J. Müller, and A. Thompson (2000), Atmospheric sulfur cycle simulated in the global model GOCART: Model description and global properties, *J. Geophys. Res.*, *105*, 24,671–24,687, doi:10.1029/2000JD900384.

Chou, C., O. Stetzer, E. Weingartner, Z. Juranyi, Z. Kanji, and U. Lohmann (2011), Ice nuclei properties within a Saharan dust event at the Jungfraujoch in the Swiss Alps, *Atmos. Chem. Phys.*, *11*, 4725–4738.

Cohard, J., and J. Pinty (2000), A comprehensive two-moment warm microphysical bulk scheme. II: 2D experiments with a non hysrostatic model, *Q. J. R. Meteorol. Soc.*, *126*, 1843–1859.

Collaud Coen, M., E. Weingartner, D. Schaub, C. Hueglin, C. Corrigan, S. Henning, M. Schwikowski, and U. Baltensperger (2004), Saharan dust events at Jungfraujoch: Detection by wavelength dependence of the single scattering albedo and first climatology analysis, *Atmos. Chem. Phys.*, *4*, 2465–2480.

Crumeyrolle, S., L. Gomes, P. Tulet, A. Matsuki, A. Schwarzenboeck, and K. Crahan-Kaku (2008), Increase of the aerosol hygroscopicity by cloud processing in a mesoscale convective system: A case study from the AMMA campaign, *Atmos. Chem. Phys.*, *8*(23), 6907–6924.

Crumeyrolle, S., H. Manninen, K. Sellegri, G. Roberts, M. Kulmala, R. Weigel, P. Laj, and A. Scharzenboeck (2010), New particle formation events measured on board the ATR-42 during the EUCAARI campaign, *Atmos. Chem. Phys.*, *10*, 6721–6735.

DeMott, P., K. Sassen, M. Poellot, D. Baumgardner, D. Rogers, S. Brooks, A. Prenni, and S. Kreidenweis (2003), African dust aerosols as atmospheric ice nuclei, *Geophys. Res. Lett.*, *30*(14), 1732, doi:10.1029/2003GL017410.

Dubovik, O., A. Smirnov, B. Holben, M. King, Y. Kaufman, T. Eck, and I. Slutsker (2000), Accuracy assessments of aerosol optical properties retrieved from Aerosol Robotic Network (AERONET) Sun and sky radiance measurements, *J. Geophys. Res.*, *105*, 9791–9806, doi:10.1029/2000JD900040.

Eck, T., B. Holben, J. Reid, O. Dubovik, A. Smirnov, N. O'Neill, I. Slutsker, and S. Kinne (1999), Wavelength dependence of the optical depth of biomass burning, urban and desert dust aerosols, *J. Geophys. Res.*, *104*, 31,333–31,349, doi:10.1029/1999JD900923.

El-Metwally, M., S. Alfaro, M. A. Wahab, and B. Chatenet (2008), Aerosol characteristic over urban Cairo: Seasonal variations as retrieved from sunphotometer measurements, *J. Geophys. Res.*, *113*, D14219, doi:10.1029/2008JD009834.

Engelstaedter, S., and R. Washington (2007), Atmospheric controls on the annual cycle of North African dust, *J. Geophys. Res.*, *112*, D03103, doi:10.1029/2006JD007195.

Engelstaedter, S., I. Tegen, and R. Washington (2006), North African dust emission and transport, *Earth Sci. Rev.*, *79*, 73–100.

Fouquart, Y., and B. Bonnel (1980), Computation of solar heating of the Earth's atmosphere: A new parametrization, *Contrib. Atmos. Phys.*, *53*, 35–62.

Franzen, L., M. Hjelmroos, P. Kallberg, E. Brorstrom-Lunden, S. Juntto, and A. Savolainen (1994), The 'yellow snow' episode of Northern Fennoscandia, March 1991—A case study of long distance transport of soil, pollen and stable organic compounds, *Atmos. Environ.*, *28*, 3587–3604.

Ginoux, P., J. Prospero, O. Torres, and M. Chin (2004), Long-term simulation of global distribution with the GOCART model: Correlation with North Atlantic oscillation, *Environ. Modell. Software*, *19*, 113–128.

Gobbi, G., F. Barnaba, R. Giorgi, and A. Santacasa (2000), Altitude-resolved properties of a Saharan dust event over the Mediterranean, *Atmos. Environ.*, *34*, 5119–5127.

Goudie, A., and N. Middelton (2001), Saharan dust storms: Nature and consequences, *Earth Sci. Rev.*, *56*, 179–204.

Grini, A., P. Tulet, and L. Gomes (2006), Dusty weather forecast using the MesoNH atmospheric model, *J. Geophys. Res.*, *111*, D19205, doi:10.1029/2005JD007007.

Hamburger, T., et al. (2011), Overview of the synoptic and pollution situation over Europe during the EUCAARI-LONGREX field campaign, *Atmos. Chem. Phys.*, *11*, 1065–1082.

Hamonou, E., P. Chazette, D. Bali, F. Dulac, X. Shneider, F. Galani, G. Ancellet, and A. Papayannis (1999), Characterization of the vertical structure of the Saharan dust transport to the Mediterranean basin, *J. Geophys. Res.*, *104*(D22), 22,257–22,270, doi:10.1029/1999JD900257.

Herman, J., and E. Celarier (1997), Earth surface reflectivity climatology at 340–380 nm from TOMS data, *J. Geophys. Res.*, *102*(D23), 28,003–28,011, doi:10.1029/97JD02074.

Herman, J., P. Bhartia, O. Torres, C. Hsu, C. Seftor, and E. Celarier (1997), Global distribution of UV-absorbing aerosols from Nimbus 7/TOMS data, *J. Geophys. Res.*, *102*(D14), 16,911–16,922, doi:10.1029/96JD03680.

Holben, B., et al. (1998), AERONET—A federated instrument network and data archive for aerosol characterization, *Remote Sens. Environ.*, *66*, 1–16.

Hsu, N., J. Herman, O. Torres, B. Holben, D. Tanre, T. Eck, A. Smirnov, B. Chatenet, and F. Lavenu (1999), Comparisons of the TOMS Aerosol Index with sunphotometer aerosol optical thickness: Result and applications, *J. Geophys. Res.*, *104*, 6269–6279, doi:10.1029/1998JD200086.

Huffman, G., R. Alder, D. Bolvin, G. Gu, E. Nelkin, K. Bowman, Y. Hong, E. Stocker, and D. Wolf (2007), The TRMM multi-satellite precipitation analysis: Quasi-global, multi-year, combined-sensor precipitation estimate a fine scales, *J. Hydrometeorol.*, *8*, 38–55.

Intergovernmental Panel on Climate Change (2001), *Climate Change 2001: The Scientific Basis*, edited by J. T. Houghton et al., Cambridge Univ. Press, Cambridge, U. K.

Israelevich, P., Z. Levin, J. Joseph, and E. Ganor (2002), Desert aerosol transport in the Mediterranean region as inferred from the TOMS aerosol index, *J. Geophys. Res.*, *107*(D21), 4572, doi:10.1029/2001JD002011.

Israelevich, P., E. Ganor, Z. Levin, and J. Joseph (2003), Annual variations of physical properties of desert dust over Israel, *J. Geophys. Res.*, *108*(D13), 4381, doi:10.1029/2002JD003163.

Joseph, J., W. Wiscombe, and J. Weinman (1976), The delta-Eddington approximation for radiative flux transfer, *J. Atmos. Sci.*, *33*, 2452–2459.

Kain, J., and J. Fritsch (1993), Convective parameterization for mesoscale models: The Kain-Fitsch scheme, in *The Representation of Cumulus Convection in Numerical Models*, *AMS Monogr. Ser.*, vol. 46, edited by K. A. Emanuel and D. J. Raymond, pp. 165–170, Am. Meteorol. Soc., Providence, R. I.

Kim, D., M. Chin, H. Yu, T. Eck, A. Smirnov, and B. Holben (2011), Dust optical properties over North Africa and Arabian Peninsula derived from the AERONET dataset, *Atmos. Chem. Phys.*, *11*, 10,733–10,741.

Koren, I., J. H. Joseph, and P. L. Israelevich (2003), Detetction of dust plumes and their sources in northeastern Libya, *Can. J. Remote Sens.*, *29*(6), 792–796.

Kubilay, N., T. Cokacar, and T. Oguz (2003), Optical properties of mineral dust outbreak over the northeastern Mediterranean, *J. Geophys. Res.*, *108*(D21), 4666, doi:10.1029/2003JD003798.

Kulmala, M., et al. (2009), Introduction: European integrated project on aerosol cloud climate and air quality interactions (EUCAARI) integrating aerosol research from nano to global scales, *Atmos. Chem. Phys.*, *9*(23), 2825–2841.

Lafore, J., et al. (1998), The Meso-NH atmospheric simulation system. Part I: Adiabatic formulation and control simulations, *Ann. Geophys.*, *16*, 90–109.

Levelt, P., et al. (2000), Science requirements document for OMI-EOS, *Rep. RS-OMIE-KMNI-001*, KMNI, De Bilt, Netherlands.

Levin, Z., E. Ganor, and V. Gladstein (1996), The effects of desert particles coated with sulfate on rain formation in the eastern Mediterranean, *J. Appl. Meteorol.*, *35*, 1511–1523.

Mahowald, N., R. Bryant, J. D. Corra, and L. Steinberger (2003), Ephemeral lakes and dust sources, *Geophys. Res. Lett.*, *30*(2), 1074, doi:10.1029/2002GL016041.

Mallet, M., P. Tulet, D. Serça, F. Solmon, O. Dubovik, J. Pelon, F. Lohou, O. Thouron, and V. Pont (2009), Impact of dust aerosols on the radiative budget, surface heat fluxes, heating rate profiles and convective activity over West Africa during March 2006, *Atmos. Chem. Phys.*, *9*, 7143–7160, doi:10.5194/acp-9-7143-2009.

Marticorena, B., and G. Bergametti (1995), Modeling the atmospheric dust cycle: 1. Design of a soil derived dust emission scheme, *J. Geophys. Res.*, *100*, 16,415–16,430, doi:10.1029/95JD00690.

Matthias, V., et al. (2004), Vertical aerosol distribution over Europe: Statistical analysis of Raman lidar data from 10 European Aerosol Research Lidar Nnetwork (EARLINET) stations, *J. Geophys. Res.*, *109*, D18201, doi:10.1029/2004JD004638.

Mattis, I., A. Ansmann, D. Müller, U. Wandinger, and D. Althausen (2002), Dual-wavelength raman lidar observations of the extinction-to-backscatter ratio of Saharan dust, *Geophys. Res. Lett.*, *29*(9), 1306, doi:10.1029/2002GL014721.

Mattis, I., D. Müller, A. Ansmann, U. Wandinger, J. Preißler, P. Seifert, and M. Tesche (2008), Ten years of multiwavelength Raman lidar observations of free-tropospheric aerosol layers over central Europe: Geometrical properties and annual cycle, *J. Geophys. Res.*, *113*, D20202, doi:10.1029/2007JD009636.

McConnell, C., E. Highwood, E. Coe, P. Formenti, B. Anderson, S. Osborne, S. Nava, K. Desboeuf, G. Chen, and M. Harrison (2008), Seasonal variations of the physical and optical characteristic of Saharan dust: Results from the Dust Outflow and Deposition to the Ocean (DODO) experiment, *J. Geophys. Res.*, *113*, D14S05, doi:10.1029/2007JD009606.

Mona, L., A. Amodeo, M. Pandofi, and G. Pappalardo (2006), Saharan dust intrusion in the Mediterranean area: Three years of Raman lidar measurements, *J. Geophys. Res.*, *111*, D16203, doi:10.1029/2005JD006569.

Morcrette, J., and Y. Fouquart (1986), The overlapping of cloud layers in shortwave radiation parametrization, *J. Atmos. Sci.*, *43*(4), 321–328.

Moulin, C., C. Lambert, U. Dayan, M. Ramonet, P. Bouquet, M. Legrand, Y. Balkansky, W. Guelle, B. Marticorena, and F. Dulac (1998), Satellite climatology of African dust transport in the Mediterranean atmosphere, *J. Geophys. Res.*, *103*(D11), 137–144, doi:10.1029/98JD00171.

Müller, D., I. Mattis, U. Wandinger, A. Ansmann, D. Althausen, O. Dubovik, S. Eckhardt, and A. Stohl (2003), Saharan dust over a central European EARLINET-AERONET site: Combined observations with Raman lidar and sunphotometer, *J. Geophys. Res.*, *108*(D12), 4345, doi:10.1029/2002JD002918.

Noihlan, J., and J. Mahfouf (1996), The ISBA land surface parametrization scheme, *Global Planet. Change*, *13*, 145–159.

Papayannis, A., et al. (2008), Systematic lidar observations of Saharan dust over Europe in the frame of EARLINET (2000–2002), *J. Geophys. Res.*, *113*, D10204, doi:10.1029/2007JD009028.

Pappalardo, G., et al. (2010), EARLINET correlative measurements for CALIPSO: First intercomparison results, *J. Geophys. Res.*, *115*, D00H19, doi:10.1029/2009JD012147.

Perrone, M. R., M. Santese, A. Tafuro, B. Holben, and A. Smirnov (2005), Aerosol load characterization over south-east Italy for one year of AERONET sunphotometer measurements, *Atmos. Res.*, *75*, 111–133.

Petzold, A., et al. (2009), Saharan dust absorption and refractive index from aircraft-based observations during SAMUM 2006, *Tellus, Ser. B*, *61*, 118–130.

Pinty, J., and P. Jabouille (1998), A mixed-phase cloud parameterization for use in mesoscale non hydrostatic model: Simulations of a squall line and of orographic precipitations, paper presented at Conference of Cloud Physics, Am. Meteorol. Soc., Everett, Wash.

Prospero, J., P. Ginoux, O. Torres, S. Nicholson, and T. Gill (2002), Environmental characterization of global sources of atmospheric soil dust identified with the Nimbus 7 Total Ozone Mapping Spectrometer (TOMS) absorbing aerosol product, *Rev. Geophys.*, *40*(1), 1002, doi:10.1029/2000RG000095.

Raut, J., and P. Chazette (2009), Assessment of vertically-resolved PM10 from mobile lidar observations, *Atmos. Chem. Phys.*, *9*, 8617–8638.

Reiff, J., G. Forbes, F. Spieksma, and J. Reynders (1986), African dust reaching north-western Europe: A case study to verify trajectory calculations, *J. Clim. Appl. Meteorol.*, *25*, 1543–1567.

Rosenfeld, D., Y. Rudich, and R. Lahav (2002), Desert dust suppressing precipitation: A possible desertification loop, *Proc. Natl. Acad. Sci. U. S. A.*, *98*, 5975–5980.

Sassen, K. (2002), Indirect climate forcing over the western US from Asian dust storm, *Geophys. Res. Lett.*, *29*(10), 1465, doi:10.1029/2001GL014051.

Sassen, K., P. DeMott, J. Prospero, and M. Poellot (2003), Saharan dust storms and indirect aerosol effects on clouds: Crystal-FACE results, *Geophys. Res. Lett.*, *30*(12), 1633, doi:10.1029/2003GL017371.

Schaap, M., A. Apituley, R. Timmermans, R. Koelemeijer, and G. de Leeuw (2009), Exploring the relation between aerosol optical depth and PM2.5 at Cabauw, the Netherlands, *Atmos. Chem. Phys.*, *9*, 909–925.

Seifert, P., S. Gross, A. Ansmann, V. Freudenthaler, A. Hiebsch, J. Schmidt, F. Schnell, M. Tesche, and M. Wiegner (2010), Heterogeneous ice nucleation in the ash plume of Eyjafjoll observed at two central European EARLINET lidar sites, paper presented at 13th Conference on Cloud Physics, Am. Meteorol. Soc., Portland, Oreg.

Slinn, W. (1979), Atmospheric sciences and power production: Precipitation scavenging, report, U.S Dep. of Energy, Washington, D. C.

Suhre, K., et al. (1998), Physico-chemical modeling of the First Aerosol Characterization Experiment (ACE 1) Lagrangian B: 1. A moving column approach, *J. Geophys. Res.*, *103*(D13), 16,433–16,455, doi:10.1029/98JD00821.

Sullivan, R. C., M. Moore, M. Petters, S. Kreidenweis, G. Roberts, and K. Prather (2009), Timescale for hygroscopic conversion of calcitemineral particles through heterogeneous reaction with nitric acid, *Phys. Chem. Chem. Phys.*, *11*, 7826–7837, doi:10.1039/B904217B.

Todd, M., et al. (2008), Quantifying uncertainty in estimates of mineral dust flux: An intercomparison of model performance over the Bodélé Depression, northern Chad, *J. Geophys. Res.*, *113*, D24107, doi:10.1029/2008JD010476.

Torres, O., P. Bhartia, J. Herman, and Z. Ahmad (1998), Derivation of aerosol properties from satellite measurements of backscattered ultraviolet radiation: Theoretical basis, *J. Geophys. Res.*, *103*, 99–110, doi:10.1029/98JD00900.

Torres, O., P. Barthia, J. Herman, A. Sinyuk, and B. Holben (2002), A long term record of aerosol optical thickness from TOMS observations and comparison to AERONET measurements, *J. Atmos. Sci.*, *59*, 398–413.

Tost, H., P. Jockel, A. Kerkweg, R. Sander, and J. Lelieveld (2006), Technical note: A new comprehensive scavenging submodel for global atmospheric chemistry modelling, *Atmos. Chem. Phys.*, *6*, 565–574.

Tulet, P., V. Crassier, F. Cousin, K. Suhre, and R. Rosset (2005), ORILAM, a three moment lognormal aerosol scheme for mesoscale atmospheric model: Online coupling into the Meso-NH-C model and validation on the Escompte campaign, *J. Geophys. Res.*, *110*, D18201, doi:10.1029/2004JD005716.

Tulet, P., A. Grini, R. Griffin and S. Petitcol (2006), ORILAM-SOA: A computationally efficient model for predicting secondary organic aerosols in 3D atmospheric models, *J. Geophys. Res.*, *111*, D23208, doi:10.1029/2006JD007152.

Tulet, P., K. Crahan-Kahu, M. Leriche, B. Aouizerats, and S. Crumeyrolle (2010), Mixing of dust aerosols into a mesoscale convective system generation, filtering and possible feedbacks on ice anvils, *Atmos. Res.*, *96*, 302–314.

Veihlmann, B., P. Levelt, P. Stammes, and J. Veefkind (2007), Simulation study of the aerosol information content in omi spectral reflectance measurements, *Atmos. Chem. Phys.*, *7*, 3115–3127.

Westphal, D., O. Toon, and N. Carlson (1987), A two dimensional numerical investigation of the dynamics and microphysics of Saharan dust storm, *J. Geophys. Res.*, *92*(D3), 3027–3049, doi:10.1029/JD092iD03p03027.

Zender, C., H. Bian, and D. Newman (2003), Mineral Dust Entrainment and Deposition (DEAD) model: Description and global dust distribution, *J. Geophys. Res.*, *108*(D14), 4416, doi:10.1029/2002JD002775.